Role of eyewall and rainband eddy forcing in tropical cyclone intensification

Ping. Zhu[1], Bryce Tyner[1], Jun A. Zhang[3,4], Eric Aligo[2], Sundararaman Gopalakrishnan[3], Frank D. Marks[3], Avichal Mehra[2], Vijay Tallapragada[2],

[1]Department of Earth and Environment, Extreme Event Institute, Florida International University, Miami, FL 33199, US
[2]Environmental Modeling Center, NCEP, NOAA, College Park, MD 20740, US
[3]Hurricane Research Division, AOML, NOAA, Miami, FL 33149, US
[4]Cooperative Institute for Marine and Atmospheric Studies, University of Miami, Miami, FL 33149, US

Correspondence to: Ping Zhu (zhup@fiu.edu)

Abstract. The fundamental mechanism underlying tropical cyclone (TC) intensification may be understood from the conservation of absolute angular momentum, where the primary circulation of a TC is driven by the torque acting on air parcels resulting from asymmetric eddy processes, including turbulence. While turbulence is commonly regarded as a flow feature pertaining to the planetary boundary layer (PBL), intense turbulent mixing generated by cloud processes also exists above the PBL in the eyewall and rainbands. Unlike the eddy forcing within the PBL that is negative definite, the sign of eyewall/rainband eddy forcing above the PBL is indefinite and thus provides a possible mechanism to spin up a TC vortex. In this study, we show that the Hurricane Weather Research & forecasting (HWRF) model, one of the operational models used for TC prediction, is unable to generate appropriate sub-grid-scale (SGS) eddy forcing above the PBL due to lack of consideration of intense turbulent mixing generated by the eyewall and rainband clouds. Incorporating an in-cloud turbulent mixing parameterization in the PBL scheme notably improves HWRF's skills on predicting rapid changes in intensity for several past major hurricanes. While the analyses show that the SGS eddy forcing above the PBL is only about one-fifth of the model-resolved eddy forcing, the simulated TC vortex inner-core structure and the associated model-resolved eddy forcing exhibit a substantial dependence on the parameterized SGS eddy processes. The results highlight the importance of eyewall/rainband SGS eddy forcing to numerical prediction of TC intensification, including rapid intensification at the current resolution of operational models.

1. Introduction

Producing timely and accurate intensity forecasts of tropical cyclones (TCs) continues to be one of the most difficult challenges in numerical weather prediction. The difficulty stems from the fact that TC intensification is not only modulated by environmental conditions (e.g., vertical wind shear) and underlying sea surface temperature (SST), but also largely depends on TC internal dynamics that involve complicated interactions of physical processes spanning over a spectrum of

scales (Marks and Shay 1998). Since numerical models use discretized grids to simulate the continuous atmosphere, the processes with scales smaller than model grid spacing, known as sub-grid scale (SGS) processes, cannot be resolved by models. Because of the high nonlinearity of the atmospheric system, the SGS processes result in new high-order terms in the grid-box-mean governing equations of the atmosphere. These new high-order terms cause the otherwise closed system no

5 longer to be closed. To close the system, additional equations that govern high-order terms need to be derived. This is the notorious closure problem of any turbulent fluid system. In practice, the high-order terms are determined parametrically in terms of model-resolved grid-box mean variables. In the atmosphere, since turbulence is a major mechanism to generate SGS perturbations, the parameterization that determines the new high-order terms is often called the turbulent mixing parameterization. Also, since turbulence is a basic flow feature pertaining to the planetary boundary layer (PBL), a turbulent

10 mixing scheme is commonly known as the PBL scheme.

The mechanism underlying TC intensification associated with TC internal dynamics including SGS processes may be best understood in a cylindrical coordinate with its origin set at the center of a TC vortex. The governing equation for the azimuthal-mean model-resolved tangential velocity of a TC may be written as:

$$\frac{\partial \bar{\tilde{v}}}{\partial t} + \bar{\tilde{u}}\frac{\partial \bar{\tilde{v}}}{\partial r} + \bar{\tilde{w}}\frac{\partial \bar{\tilde{v}}}{\partial z} = -\bar{\tilde{u}}\left(f + \frac{\bar{\tilde{v}}}{r}\right) + F_\lambda + F_{sgs\_\lambda}, \qquad F_\lambda = -\overline{\tilde{u}'\frac{\partial \tilde{v}'}{\partial r}} - \overline{\tilde{v}'\frac{\partial \tilde{v}'}{r\partial \lambda}} - \overline{\tilde{w}'\frac{\partial \tilde{v}'}{\partial z}} - \frac{\overline{\tilde{u}'\tilde{v}'}}{r}, \qquad (1)$$

15 where r, λ, and z represent the radial, azimuthal, and vertical coordinate axes; $\tilde{u}$, $\tilde{v}$, and $\tilde{w}$, are the model-resolved radial, tangential, and vertical wind components, respectively; f is Coriolis parameter. Overbar and prime indicate the azimuthal-mean and the perturbation away from the azimuthal-mean; F_λ is the azimuthal-mean tangential eddy correlation term resulting from the model-resolved asymmetric eddy processes; and F_{sgs_λ} is the azimuthal-mean tangential SGS tendency resulting from the parameterized eddy processes (or turbulence). In the PBL, eddy forcing $F_\lambda + F_{sgs\_\lambda}$ is negative definite,

20 meaning that it always slows down the motion; thus, it physically represents the frictional force in the tangential direction. Defining the model-resolved tangential absolute angular momentum per unit mass as $\bar{\tilde{M}} = r\bar{\tilde{v}} + \frac{1}{2}fr^2$, then, it is easy to show that the azimuthal-mean tangential wind budget equation, Eq.(1), can be rewritten as:

$$\frac{D\bar{\tilde{M}}}{Dt} = \frac{\partial \bar{\tilde{M}}}{\partial t} + \bar{\tilde{u}}\frac{\partial \bar{\tilde{M}}}{\partial r} + \bar{\tilde{w}}\frac{\partial \bar{\tilde{M}}}{\partial z} = r(F_\lambda + F_{sgs\_\lambda}), \qquad (2)$$

where $\frac{D\bar{\tilde{M}}}{Dt} = \frac{\partial \bar{\tilde{M}}}{\partial t} + \bar{\tilde{u}}\frac{\partial \bar{\tilde{M}}}{\partial r} + \bar{\tilde{w}}\frac{\partial \bar{\tilde{M}}}{\partial z}$ is the material derivative following air particles along the model-resolved axisymmetric flow

25 and $r(F_\lambda + F_{sgs\_\lambda})$ is the torque per unit mass acting on air parcels resulting from the model-resolved and SGS eddy forcing. For $F_\lambda + F_{sgs\_\lambda} = 0$, $\bar{\tilde{M}}$ is materially conserved. As air parcels move radially inward (decrease of r), they must spin up in order to conserve their absolute angular momentum. Conversely, air parcels must spin down as they move radially outward. Thus, spin-up or spin-down of a TC vortex (e.g., increase or decrease of $\bar{\tilde{v}}$) in an inviscid flow requires azimuthal-mean radial flow. In other words, the evolution of the primary circulation of a TC vortex must be accompanied by a secondary

overturning circulation. Physically, this overturning circulation is induced by friction within the PBL and diabatic heating of convection.

To date, TC intensification is commonly considered as a cooperative process among the primary and secondary circulations, convection, PBL processes, and air-sea interaction. Latent heating from ocean surface evaporation serving as the ultimate

5   energy source for TCs had been identified early in the 1950s (Kleinschmidt 1951; Riehl 1954). Both the Conditional Instability of the Second Kind (CISK) and cooperative-intensification mechanism (Ooyama 1982), the two early theories for TC intensification, recognized the role of the PBL in converging moisture to sustain deep convection of a TC. Charney and Eliassen (1964) stated, "Friction performs a dual role; it acts to dissipate kinetic energy, but because of the frictional convergence in the moist surface boundary layer, it acts also to supply latent heat energy to the system". But it was

10 Emanuel's Wind-Induced Surface Heat Exchange (WISHE, Emanuel 1986) theory that first recognized the critical role of air-sea interaction in the intensification process. While the aforementioned TC theories plus the more advanced three-dimensional rotating convective updraft paradigm (Montgomery and Smith 2014) recognized the critical role of PBL in TC intensification, they all treated the PBL as a shallow turbulent layer adjacent to Earth's surface with a depth typically less than 1 km. By doing so, they implicitly adopted the basic assumptions of the classic PBL theory: (1) turbulent mixing is

15 responsible for the vertical transport of momentum, heat, and moisture; (2) the mean vertical velocity in the PBL is negligible; and (3) vertical turbulent transport becomes negligible above the PBL. However, turbulence and the resultant turbulent transport and turbulent kinetic energy (TKE) cannot always be neglected above the PBL. Intense turbulent mixing within the deep convective clouds has been widely observed by aircraft, Doppler radar/lidar, and other advanced remote sensing instruments (e.g., LeMone and Zipser 1980; Marks et al. 2008; Hogan et al. 2009; Giangrande et al. 2013). In

20 particular, using the TKE derived from the airborne radar data collected in Hurricane Rita (2005), Lorsolo et al. (2010) showed that large TKE exists above the PBL in the eyewall and rainbands. Figure 1 shows the composite of TKE derived using Lorsolo et al. (2010)'s method based on the airborne radar observations from 116 radial legs of P3 flights in the 2003-2010 hurricanes seasons. It clearly demonstrates that the intense turbulence exists above the PBL in the conventional definition all the way up to over 10 km in the eyewall.

25 Realizing the deep convective nature of TCs, Smith et al. (2008) and Smith and Montgomery (2010) warned that the conventional PBL theory may become invalid in the TC inner-core region as the low-level radial inflow ascends swiftly within the eyewall. In fact, the problem of applying conventional PBL theory to a deep convective regime had been recognized early in the 1970s and 1980s. Deardorff (1972) noted, "*The definition of PBL has not included the region of turbulence within towering cumuli but only the average height of surface induced turbulent fluxes outside of such clouds*".

30 Moss and Rosenthal (1975) added, "*The method (of defining the PBL) contains several elements that may or may not be applicable under hurricane conditions*". Shapiro (1983) wrote, "*As the radius of maximum tangential wind is approached, the boundary layer itself becomes ill defined, as air is pulled up into the active convection*". Stull (1988) also acknowledged

that "*the conventional definition of PBL is not applicable to the intertropical convergence zone (ITCZ), where the air ascends into deep convective clouds*". The problem here, however, is not about how to redefine PBL to encompass all the scenarios including the deep convective regime. This is because the concept of PBL always applies as to the layer adjacent to the surface that is directly affected by the surface processes. From the perspective of TC intensification, the real question that

5   needs to be answered is: Is the intense turbulent mixing above the PBL in the eyewall and rainbands generated by cloud processes important to TC intensification? This question may be addressed by evaluating the terms in Eq. (2). In classic intensification theories, a fundamental mechanism underlying TC intensification is the conservation of absolute angular momentum. As we just pointed out, the assumption of $F_\lambda + F_{sgs\_\lambda} = 0$ above the PBL is, in fact, invalid in the eyewall and rainbands because of the eddy processes associated with convection. In this case, $F_\lambda + F_{sgs\_\lambda}$ becomes an important forcing

10   for $\bar{\bar{M}}$. Unlike $F_\lambda + F_{sgs\_\lambda}$ in the PBL, which is negative definite, the eddy forcing above the PBL resulting from eyewall and rainband convection can no longer be interpreted as the frictional force, since it has nothing to do with the surface processes. The sign of $F_\lambda + F_{sgs\_\lambda}$ in this case depends on the details of eddy processes, and thus, is indefinite. For $F_\lambda + F_{sgs\_\lambda} > 0$, $\bar{\bar{M}}$ increases with time following the air parcels, indicating that eddy processes of eyewall and rainband convection provide a mechanism to spin up a TC vortex. This argument is consistent with the vortex Rossby wave theory that eddy energy can be

15   axisymmetrized into the vortex mean flow to spin up a vortex via wave-mean-flow interaction (e.g., Montgomery and Kallenbach 1997; Persing et al. 2013). It is clear from this regard that a correct determination of eddy forcing $F_\lambda + F_{sgs\_\lambda}$ is one of the keys to the accurate prediction of TC intensity change, as it is the sole forcing for the conservation of $\bar{\bar{M}}$.

In addition to the direct tangential eddy forcing $F_\lambda + F_{sgs\_\lambda}$ to the primary circulation ($\bar{\bar{v}}$) of a TC vortex, TC intensification is also intimately involved with the secondary overturning circulation induced by friction and diabatic heating. The

20   azimuthal-mean governing equations for model-resolved radial velocity and vertical velocity of the overturning circulation may be written as:

$$\frac{D\bar{\bar{u}}}{Dt} - C = -\frac{1}{\bar{\bar{\rho}}}\frac{\partial \bar{\bar{p}}}{\partial r} + F_r + F_{sgs\_r}, \quad C = \frac{\bar{\bar{v}}^2}{r} + f\bar{\bar{v}}, \quad F_r = -\overline{\tilde{u}'\frac{\partial \tilde{u}'}{\partial r}} - \overline{\tilde{v}'\frac{\partial \tilde{u}'}{r\partial\lambda}} - \overline{\tilde{w}'\frac{\partial \tilde{u}'}{\partial z}} - \frac{\overline{\tilde{v}'^2}}{r}, \tag{3}$$

$$\frac{D\bar{\bar{w}}}{Dt} = -\frac{1}{\bar{\bar{\rho}}}\frac{\partial \bar{\bar{p}}}{\partial z} - g + F_w + F_{sgs\_w}, \qquad F_w = -\overline{\tilde{u}'\frac{\partial \tilde{w}'}{\partial r}} - \overline{\tilde{v}'\frac{\partial \tilde{w}'}{r\partial\lambda}} - \overline{\tilde{w}'\frac{\partial \tilde{w}'}{\partial z}}, \tag{4}$$

where $F_r + F_{sgs\_r}$ and $F_w + F_{sgs\_w}$ are the model-resolved and SGS eddy forcing terms in the radial and vertical direction; $\bar{\bar{p}}$

25   and $\bar{\bar{\rho}}$ are the azimuthal-mean model-resolved pressure and air density, respectively; and g is the gravitational acceleration. Differentiating Eq. (3) and Eq. (4) with respect to r and z, respectively, and then, eliminating the pressure term, it yields,

$$\frac{\partial}{\partial r}\left[\bar{\bar{\rho}}\left(\frac{D\bar{\bar{w}}}{Dt} + g - F_w - F_{sgs\_w}\right)\right] + \frac{\partial}{\partial z}\left[\bar{\bar{\rho}}\left(-\frac{D\bar{\bar{u}}}{Dt} + C + F_r + F_{sgs\_r}\right)\right] = 0. \tag{5}$$

Using equation of state and definition of potential temperature θ, with some algebraic derivations, Eq. (5) can be rewritten in terms of $\chi = \frac{1}{\theta}$,

$$\frac{\partial}{\partial r}\left[\bar{\tilde{\chi}}\left(\frac{D\bar{\tilde{w}}}{Dt} + g - F_w - F_{sgs\_w}\right)\right] + \frac{\partial}{\partial z}\left[\bar{\tilde{\chi}}\left(-\frac{D\bar{\tilde{u}}}{Dt} + C + F_r + F_{sgs\_r}\right)\right] = 0, \tag{6}$$

where χ is determined by the heat conservation equation,

$$\frac{\partial\bar{\tilde{\chi}}}{\partial t} + \bar{\tilde{u}}\frac{\partial\bar{\tilde{\chi}}}{\partial r} + \bar{\tilde{w}}\frac{\partial\bar{\tilde{\chi}}}{\partial z} = -\bar{\tilde{\chi}}^2(\dot{\theta} + F_\theta + F_{sgs\_\theta}), \tag{7}$$

where F_θ and F_{sgs_θ} are the model-resolved and SGS eddy forcing for heat, respectively; and $\dot{\theta}$ is the diabatic heating. In numerical simulations, Eq. (6) is the equation that governs the azimuthal-mean overturning circulation of a TC vortex.

In the classic TC theories, the acceleration of the overturning circulation and radial/vertical eddy forcings ($F_r + F_{sgs\_r}$, $F_w + F_{sgs\_w}$) are neglected, i.e., a TC vortex is assumed to satisfy the gradient wind balance ($C = \frac{1}{\bar{\rho}}\frac{\partial\bar{p}}{\partial r}$) and hydrostatic balance ($-\frac{1}{\bar{\rho}}\frac{\partial\bar{p}}{\partial z} - g = 0$). Then, Eq. (6) simplifies to the well-known thermal wind relationship,

$$g\frac{\partial\tilde{\chi}}{\partial r} + \frac{\partial(\tilde{\chi}C)}{\partial z} = 0. \tag{8}$$

Differentiating Eq. (8) with respect to time, eliminating the time derivatives of $\bar{\tilde{\chi}}$ and $\bar{v}$ using Eq. (1) and Eq. (7), and then, combining the azimuthal-mean continuity equation that allows the azimuthal-mean radial and vertical velocity to be expressed in terms of a streamfunction, an analytical expression of the overturning circulation known as Sawyer-Eliassen equation can be derived (e.g., Shapiro and Willoughby 1982; Smith et al. 2005, Bui et al. 2009). While this balanced model successfully considers the tangential and thermodynamic eddy forcing and captures the basic characteristics of the overturning circulation, it neglects the important radial and vertical eddy forcing aloft associated with deep convection and PBL turbulence in the eyewall and rainbands. Therefore, intensification theories built upon gradient wind balance and hydrostatic balance may lack the ability to explain rapid intensity changes driven by the internal dynamics when radial and vertical eddy forcing is important.

Numerical models built upon primitive equations presumably have the ability to capture eddy forcing associated with convection and PBL turbulence. Advances in computer technology nowadays have reduced model horizontal grid spacing of operational models down to 1-2 km. While higher resolution models allow dynamic eddy forcing (F_λ, F_r, F_w) and thermodynamic eddy forcing for heat and moisture (F_θ, F_q) to be better resolved in numerical simulations, it remains to be poorly understood as to what governs the sign, magnitude, and radius-height distribution of eddy forcings above the PBL. Leaving aside the question if high resolution numerical models can generate robust model-resolved eddy forcing, a source of uncertainty in intensity forecast arises from the parametric determination of SGS eddy forcing.

In numerical models, the SGS forcings (F_{sgs_λ}, F_{sgs_r}, F_{sgs_w}, F_{sgs_θ}, and F_{sgs_q}) are determined by the turbulent mixing scheme. Current effort mainly focuses on the improvement of parameterization of turbulent mixing within the PBL. The importance of eyewall/rainband SGS eddy forcing above the PBL to TC intensification has been largely overlooked in the

past for a few reasons. First, the critical role of radial inflow, PBL processes, and surface latent heating in maintaining and intensifying a TC vortex has overshadowed the importance of the SGS forcing aloft associated with eyewall/rainband convection. Second, unlike turbulence in the PBL, which has a solid theory built upon observations, turbulence aloft in deep convection is difficult to access. Lack of observations largely limits our understanding of the in-cloud turbulent mixing

5   processes and the resultant SGS eddy forcing to the momentum and heat budgets of a TC. Third, for deep convection, the focus is on the cumulus parameterization. But cumulus schemes are not designed to account for the eddy forcing to the momentum, heat, and moisture budgets but rather serve as a means to remove the convective instability generated by the large-scale flow and alter the thermodynamic structure of the environment based on the parameterized convective fluxes and precipitation (Arakawa and Schubert 1974; Wu and Arakawa 2014). It is commonly assumed and widely accepted that the

10   coherent up-/down-drafts take the central role in establishing the equilibrium between the generation of moist convective instability by the environmental processes and the stabilization of environment by cumulus convection. The effect of small scale turbulence is negligible in this perspective. But the contribution of in-cloud turbulence to eddy forcing in TC intensification is unknown. Finally, almost all turbulent mixing schemes used today for TC prediction were originally developed to represent turbulent processes within the PBL in fair-weather conditions in which the turbulent PBL is cleanly

15   separated from the free atmosphere above by a capping inversion. Often in these schemes, a simple method based on the bulk Richardson number is adopted to account for the free atmosphere turbulence if there is any (e.g., Hong and Pan, 1996). These schemes may lack the ability to represent the in-cloud turbulence in the eyewall and rainbands generated by the cloud processes.

In this study, using numerical simulations by the Hurricane Weather Research and Forecast (HWRF) modeling system, one

20   of the operational models used for TC prediction at the Environmental Modeling Center (EMC), NOAA, we investigate the role of eyewall/rainband eddy forcing in governing TC intensity change, in particular, rapid intensification (RI). We demonstrate the importance of in-cloud turbulent mixing parameterization to generation of robust eyewall/rainband eddy forcing in numerical simulations. This paper is organized as follows. In section 2, we show problems associated with the turbulent mixing scheme used in the operational HWRF in representing eyewall/rainband in-cloud turbulence and discuss

25   methods of how to incorporate the parameterization of in-cloud turbulence with the PBL scheme used in HWRF. The simulation results by HWRF with the operational setting and the modified PBL scheme that includes in-cloud turbulent mixing parameterization are presented in section3 followed by a summary and in section 4.

2. HWRF PBL scheme and in-cloud turbulent mixing parameterization

The numerical model used in this study is the operational HWRF version 3.8a. It consists of triple-nested domains on an E-

30   grid. The grid-spacing of the three domains is 0.135^0, 0.045^0, and 0.015^0 degree, corresponding approximately to 18 km, 6 km, and 2 km, respectively. There are 61 levels in the vertical. The details of HWRFv3.8a release can be accessed at https://dtcenter.org/HurrWRF/users/docs/index.php. Since this study focuses on the role of internal eyewall/rainband eddy

forcing in TC intensification, to avoid the complication from the interactive underlying ocean, all simulations presented in this paper were performed by the uncoupled atmospheric model of HWRF. The initial and boundary conditions for the real-case TC simulations were supplied by the Global Forecast System (GFS) data.

As discussed in the previous section, in numerical models the SGS eddy forcing that drives the primary and secondary circulations of a TC is determined by the turbulent mixing scheme. In the operational HWRF, the turbulent mixing is parameterized by a PBL scheme, which was coded based on the one formulated by Hong and Pan (1996). It is a typical K-closure (or first-order-closure) turbulent mixing scheme. Although there have been modifications to the scheme throughout the years, the basic formulae used to determine eddy exchange coefficients are kept the same as those originally proposed by Hong and Pan (1996). In this scheme, the eddy exchange coefficients are determined separately based on the diagnosed PBL height. Within the PBL, the momentum eddy viscosity is calculated as:

$$K_m = \kappa \frac{u_*}{\phi_m} \alpha z (1 - \frac{z}{h})^2, \tag{9}$$

where κ is the von Karman constant, u_* is the friction velocity, z is the height above the ground surface, ϕ_m is the surface layer stability function obtained by Businger et al. (1971), and h is the diagnosed PBL height calculated iteratively based on the bulk Richardson number over the PBL depth and the buoyancy of surface-driven thermals. Although there are many sophisticated methods to parameterize SGS turbulent mixing, such as TKE closure, high-order closure, nonlocal mixing, and schemes formulated using variables conserved for moist reversible adiabatic processes, the K-closure scheme is arguably the best choice for operational models at the current stage as it requires less computational resource. However, Eq. (9) was originally formulated to account for PBL turbulent mixing in non-TC conditions (Troen and Mahrt 1986; Holtslag et al. 1990; Holtslag and Boville 1993). Observations from multiple TCs by Zhang et al. (2011) showed that Eq. (9) substantially overestimates the eddy viscosity in the PBL. In light of this finding, Gopalakrishnan et al. (2013) introduced a coefficient α ($0 < \alpha < 1$) in Eq. (9) to reduce eddy viscosity in TC simulations. This tuning of eddy viscosity via α now has been adopted in the operational HWRF. Above the diagnosed PBL height, the momentum eddy viscosity is calculated as:

$$K_m = l^2 f_m(Ri_g) \sqrt{\left|\frac{\partial \tilde{u}}{\partial z}\right|^2 + \left|\frac{\partial \tilde{v}}{\partial z}\right|^2}, \tag{10}$$

where l is the mixing length, $f_m(Ri_g)$ is the stability function of gradient Richardson number, $Ri_g = \frac{g}{\theta_0} \frac{\partial \widetilde{\theta_v}}{\partial x} / (\left|\frac{\partial \tilde{u}}{\partial z}\right|^2 + \left|\frac{\partial \tilde{v}}{\partial z}\right|^2)$, and $\sqrt{\left|\frac{\partial \tilde{u}}{\partial z}\right|^2 + \left|\frac{\partial \tilde{v}}{\partial z}\right|^2}$ is the vertical wind shear. This is a method that was originally designed to account for the free-atmosphere diffusion.

For fair-weather conditions, the parameterization formulated by Eq. (9) and Eq. (10) provides a practical way to appropriately parameterize the SGS turbulent mixing within and above the PBL since the turbulent layer resulting from the surface processes is often cleanly separated from the free atmosphere by a capping inversion. The mid-point of the inversion

zone (or entrainment zone) is traditionally defined as the PBL height (Stull 1988). In a TC environment, however, turbulence is no longer solely generated by the shear production and buoyancy production associated with the surface processes; it can also be generated by cloud processes aloft due to cloud radiative cooling, evaporative cooling, and inhomogeneous diabatic heating and cooling in the clouds. Thus, although the concept of PBL height is still applicable, it becomes ambiguous from

5   the turbulent mixing perspective. In many TC studies, the PBL is defined either as the turbulent layer that is directly affected by the surface processes or as the inflow layer of the secondary circulation. But in either case, the so-defined PBL height is by no means a physical interface that separates the turbulence generated by surface processes and by cloud processes. This is particularly true in the eyewall and rainbands of a TC, where intense turbulence can extend from the surface all the way up to the upper troposphere, as was illustrated in Fig. 1. Thus, from the nature of turbulent mixing, an artificial separation of

10 turbulence using a diagnosed "PBL" height is not a physically sound method to parameterize the internally connected SGS turbulent mixing in the eyewall or any deep convective areas in a TC. Moreover, an artificial separation of the PBL from the free atmosphere above may create an unrealistic discontinuity in the vertical profile of eddy viscosity in this method. Following Eq. (9), as height z approaches the diagnosed "PBL" height h, eddy viscosity K_m becomes zero to result in zero turbulent mixing at a certain model grid level if the diagnosed PBL height falls exactly at this level. Above the diagnosed

15 PBL, the turbulent mixing jumps to whatever value estimated by Eq. (10). This singular point in the vertical profile of eddy exchange coefficient could cause problems in representing turbulent mixing in the eyewall and rainbands.

We carefully examined the eddy exchange coefficients in multiple TC simulations by the operational HWRF and found that the default PBL scheme is unable to generate intense turbulent mixing in the eyewall and rainbands. As an example, Figure 2 shows the HWRF simulated eddy exchange coefficients for momentum (K_m) at different altitudes of Hurricane Jimena

20 (2015) at an arbitrary time before the storm reached its maximum intensity. At a height within the PBL (500m), the magnitude and horizontal spatial distribution reflects well the strong turbulent mixing in the eyewall and rainbands. Above the PBL (2.0 km, 5.0 km), the HWRF generated eddy exchange coefficients are virtually zero with sporadic spikes elsewhere. This result suggests that the PBL scheme used in the operational HWRF fails to capture the intense turbulent mixing above the PBL in the deep convective eyewall and rainbands. This is not a surprise since Eq. (10) was originally

25 developed to parameterize free-atmosphere diffusion and is incapable of representing the intense turbulent mixing generated by cloud processes. We hypothesize that lack of appropriate SGS eddy forcing associated with deep convection above the PBL in the eyewall and rainbands is one of the culprits for the intensity forecast failure in many cases of HWRF forecasts, since SGS eddy forcing (F_{sgs_λ}, F_{sgs_r}, F_{sgs_w}, F_{sgs_θ}, and F_{sgs_q}) serves as a direct forcing for driving the primary and secondary circulations of a TC.

30 To better understand the characteristics of intense turbulent mixing in eyewall clouds, we performed a large eddy simulation (LES) of Hurricane Isabel (2003) in a hindcasting mode using WRF model with the Advanced Research WRF (ARW) dynamic core. The detailed procedure of configuring a WRF-LES for TC simulations can be found in Zhu (2008) and Zhu et

al. (2015). In this simulation, the innermost domain of the WRF-LES covered the entire eyewall of Isabel (2003) with a horizontal grid-spacing of 100 m. 75 levels were configured in the vertical. The simulation was initialized and forced by the NCEP FNL analyses and run for 12 hours (from 00:00 to 12:00 UTC 12 September 2003). The details and results of this Giga WRF-LES will be reported in a separate paper. Figure 3a shows the simulated surface (10-m) wind speeds of Isabel

5 after 8 simulation hours. The fine resolution allows us to quantify the vertical transport induced by the large turbulent eddies. Figures 3b-3d show the azimuthal-mean WRF-LES resolved kinematic moisture fluxes ($\overline{w'q'}$) and x-direction/y-direction kinematic momentum fluxes ($\overline{w'u'}$, $\overline{w'v'}$) computed using the eddy correlation method after 8 simulation hours. It clearly shows that (1) vertical transport by large turbulent eddies continues increasing above the PBL (defined in the conventional way) and reaches the peak in the mid-troposphere and (2) there is no discontinuity across the PBL that separates the

10 turbulence generated by the surface processes and cloud processes aloft in the eyewall.

The discussion above and the results shown in Fig. 2 and Fig. 3b suggest that to appropriately parameterize the turbulent mixing generated by cloud processes in the eyewall and rainbands, one may have to abandon the idea of using the diagnosed "PBL" height to artificially separate the internally connected turbulence generated by the surface and cloud processes. From the nature of turbulent mixing, it is more logical to treat the turbulence in the eyewall and rainbands generated by the surface

15 and cloud processes as a whole, i.e., treat the entire turbulent layer (TL) as an integrated layer. Physically, it makes sense as turbulent mixing generated by different processes in a deep convective environment cannot be artificially separated. We wish to emphasize that such a change from "PBL" to "TL" will not affect the turbulent mixing parameterization outside the deep convective area since the "TL" is virtually the same as the "PBL" in that case. The remaining question is how to appropriately define and determine a "TL" in the eyewall and rainbands.

20 One way to improve the representation of turbulent mixing in the eyewall and rainbands is to develop a physically robust scheme using more sophisticated approaches, such as, TKE, high-order, or nonlocal closure, to replace Eq. (9) and (10). However, a sophisticated method may not necessarily generate the desired results without significant tuning effort and thorough evaluation against observations, since an operational model consists of many physics modules that interact with each other and with the model dynamic core. How to integrate an individual scheme in a model to work in concert with other

25 modules is an important but difficult scientific and technical problem. To avoid possible degrading of HWRF's forecasting performance, a practical way is to keep the current framework of PBL scheme and refine it by incorporating an in-cloud turbulent mixing parameterization with the existing PBL scheme in a unified matter. Technically, this is relatively easy to do and scientifically it makes sense, since the "TL" should be the same as the "PBL" outside deep convective regions, and thus, nothing needs to be changed for the current PBL scheme used in HWRF. The only change that needs to be made is to

30 overwrite the default diagnosed PBL height in the eyewall and rainbands with a newly determined "TL" height.

Since this study focuses on the turbulence generated by the cloud processes, a simple way to determine "TL" is to link "TL" directly to model-predicted cloud properties. A natural choice of such cloud properties is the cloud radar reflectivity, a product normally available from the microphysics module of a model. In the operational HWRF version 3.8a, the Ferrier-Aligo microphysical scheme (Aligo et al. 2018) calculates radar reflectivity at each time step. Figure 4 shows an example of the horizontal spatial distribution of HWRF simulated cloud radar reflectivity at different altitudes for Hurricane Jimena (2015) at an instant time along with an individual vertical profile of radar reflectivity in the eyewall and azimuthal-mean radius-height structure of radar reflectivity. The vertical profile clearly shows that the simulated radar reflectivity in the eyewall remains nearly constant with height below the freezing level, and then, decreases sharply around 6 – 7 km in altitude. This unique feature allows us to determine "TL" from the radar reflectivity under the assumption that "TL" is virtually the cloud layer with prevalence of turbulence. After many tests, we choose 28 dBZ as a critical value to define "TL" in HWRF simulations. If no such a layer with radar reflectivity consistently greater than 28 dBZ is found or such defined "TL" is lower than the default "PBL", then, the default "PBL" is assumed to be the "TL". Thus, the change from "PBL" to "TL" will not affect the treatment of turbulent mixing elsewhere except for the diagnosed eyewall and rainbands with large reflectivity. Once "TL" is determined, the eddy exchange coefficients below and above the top of the diagnosed "TL" will be calculated following Eq. (9) and Eq. (10), respectively. To retain the HWRF predicted turbulent structure and transport within the PBL, the eddy exchange coefficients below the PBL height are, then, overwritten by the eddy exchange coefficients determined by the default diagnosed "PBL" with a smoothing applied at the top of the "PBL" so that the eddy exchange coefficients in the eyewall and rainband change continuously from the PBL to the cloud layer. Thus, nothing is changed for the HWRF PBL scheme except that the new scheme includes an in-cloud turbulent mixing parameterization in the eyewall and rainbands determined from the "TL". Figure 5 shows the simulated eddy exchange coefficients of momentum, K_m, at different altitudes of Hurricane Jimena (2015) by the HWRF with the inclusion of in-cloud turbulent mixing parameterization. The modification from "PBL" to "TL" allows HWRF to successfully capture the in-cloud turbulent mixing. The horizontal spatial distribution of K_m above the PBL well reflects the eyewall and rainband structure of the TC vortex, which is in stark contrast to the default operational HWRF that generates virtually no turbulent mixing above the PBL (Fig. 2). It should be pointed out that the method used in this study to include the effects of in-cloud turbulent mixing is crude and does not consider the specific mechanisms in generating in-cloud turbulence, and thus, the scheme in its current form may not be directly used in operational forecasts. Nonetheless, this simple modification allows us to look into and examine the role of eyewall and rainband eddy forcing above the PBL in TC intensification. An additional advantage of this change from "PBL" to "TL" allows for a possible internal interaction between microphysics and turbulence. In real TCs, cloud microphysical processes directly interact with in-cloud turbulence to generate the diabatic heating that drives the overturning circulation. The negligible turbulent mixing above the PBL in the operational HWRF virtually removes the microphysics-turbulence interaction in eyewall/rainband clouds. While simple, the inclusion of in-cloud turbulent mixing by overwriting the "PBL" height with the "TL" provides an avenue that allows microphysics to directly interact with turbulence

in simulations. In the next section, we show that such a modification improves HWRF's skills in predicting TC intensity change, in particular, RI.

3. Results

To evaluate the modified HWRF PBL scheme with the inclusion of in-cloud turbulent mixing parameterization and investigate the role of eyewall/rainband eddy forcing in modulating TC intensity change, we simulated 16 storms in the Atlantic basin and eastern tropical Pacific in the past four seasons (2014-2017) with different intensities ranging from tropical storms to major hurricanes. For each storm, we simulated 4 cycles with the model initialized at different time. These simulations allow us to provide an initial evaluation of the in-cloud turbulent mixing parameterization and address scientific issues associated with TC intensity change in different TC conditions. In this paper, we mainly focus on RI. Here, we present one of the four simulations of Hurricane Jimena (2015), which was initialized at 12:00 UTC 27 August, 2015. Using this simulation, we investigate how eyewall and rainband eddy forcing drives the RI of Jimena (2015).

Figure 6 compares the storm track and intensity from the two simulations of Jimena (2015) by HWRF using the default PBL scheme and the PBL scheme that includes in-cloud turbulent mixing parameterization along with the best track data. These two simulations are named as "DEF-HWRF" and "TL-HWRF" respectively hereafter. While DEF-HWRF does an excellent job in reproducing the observed track, it under-predicts the observed storm intensity by a large margin. The integrated turbulent mixing parameterization in the eyewall and rainbands (TL-HWRF) shows little impact on the simulated storm track but improves the intensity forecast substantially. It allows HWRF to successfully capture the observed RI of Jimena, suggesting the importance of eyewall/rainband turbulent mixing above the PBL in modulating TC intensification. In the following sections, we explore and discuss the underlying reasons for such an improvement in intensity forecast.

Figure 7 shows the Naval Research laboratory 37 GHz color image from the Advanced Microwave Scanning Radiometer 2 (AMSR2) at 20 UTC 28 August 2015, a time close to the initiation of Jimena's RI. A nearly closed ring feature around the storm center is clearly visible in the satellite image. From a large amount of 37 GHz microwave color products, Kieper and Jiang (2012) showed that the first appearance of a cyan color ring around the storm center is highly correlated to subsequent RI, provided that environmental conditions are favorable. This result is consistent with the later analyses of Tropical Rainfall Measuring Mission (TRMM) 29 Precipitation Radar (PR) data (Jiang and Ramirez 2013; and Tao and Jiang 2015), which showed that nearly 90% of RI storms in different ocean basins formed a precipitation ring around the storm center prior to RI. The relationship between the ring feature and the subsequent RI obtained from these observational studies appears to be consistent with the theoretical finding of Nolan et al. (2007), who demonstrated that the intensification processes of a balanced, baroclinic TC-like vortex is mainly driven by the TC symmetric response to the azimuthally-averaged diabatic heating, rather than to the heating directly associated with individual asymmetries distributed around the TC vortex. To see if Jimena's RI possesses the similar RI signature found in these observational and theoretical studies, we carefully examined

the inner-core structure of the simulated Jimena (2015) prior and during the early stage of RI. Figure 8 shows the horizontal distribution of simulated vertical velocity and hydrometeor mixing ratio at 5 km altitude from the two HWRF simulations with and without in-cloud turbulent mixing parameterization. There is no closed ring-like feature around the storm center shown in "DEF-HWRF". The simulated eyewall appears to be much larger in size than the satellite observed eyewall (Figs. 5   8a and 8c). It suggests that HWRF with operational model physics is unable to simulate the right vortex inner-core structure in this case, and thus, fails to generate the TC internal processes needed for the subsequent RI. In contrast, "TL-HWRF" produces a well-defined closed ring around the storm center that is clearly shown in both dynamic (vertical velocity, Fig. 8b) and thermodynamic (hydrometeor mixing ratio, Fig. 8d) fields. The size of the simulated closed ring in "TL-HWRF" is similar to that shown in the satellite image. In addition, the simulated asymmetric rainband structure with the strongest 10   convection occurring in the southeast quadrant is consistent with the satellite observation. The similar TC inner-core structure shown in "TL-HWRF" and satellite observations implies that the improvement in intensity forecast by "TL-HWRF" (Fig. 6) was not accidental or due to wrong reasons, but should be attributed to the right internal processes and storm inner-core structure captured by the simulation. It also suggests the importance of eyewall/rainband turbulent mixing above the PBL to the modulation of TC inner-core structure and intensification.

15   Figure 9 shows the simulated azimuthal-mean radius-height structure of vertical velocity, hydrometeor mixing ratio, radial inflow/outflow, and radial flow convergence averaged over the RI period from 06 UTC 28 to 06 UTC 29 August, 2015. Compared with the DEF-HWRF, TL-HWRF generated much stronger updrafts (gray contours) in the eyewall, stronger radial inflow (red contours) within the PBL, and outflow (white contours) above, which are consistent with the strong storm intensity simulated by this experiment (Fig. 6). Furthermore, in the TL-HWRF experiment, the radial flow convergence 20   (black contours) matches well with the eyewall updrafts. This feature facilitates an efficient transport of moisture into the eyewall to result in a large amount of condensate (color shading) in the eyewall. The resultant latent heating fosters the rapid converging spin-up processes as air parcels move radially inward and ascend swiftly within the eyewall. This result suggests the importance of microphysics-turbulence interaction in TC intensification. In contrast, the peaks of persistent radial flow convergence in DEF-HWRF do not occur in the eyewall, but rather extend radially outward along the interface of radial 25   inflow and outflow. Such a structure is apparently unfavourable to the rapid development of the vortex, since it cannot generate the efficient converging spin-up processes. Therefore, the simulated storm intensity difference by the two HWRFs may be largely attributed to the differences in the strength and structure of the secondary overturning circulation in this case. However, we note the depth of the radial inflow layer is similar in both HWRF simulations. It suggests that the inclusion of in-cloud turbulent mixing parameterization aloft in the simulation does not alter the basic structure of the PBL in the TC 30   vortex inner-core region.

To better understand the intensification processes in the two HWRF simulations, we examined the tangential eddy forcing $(F_\lambda + F_{sgs\_\lambda})$ that directly governs the primary circulation of the TC vortex. The model-resolved tangential eddy forcing F_λ is

calculated by Eq. (1) from the model-resolved wind fields available in the standard HWRF output. The SGS tangential eddy forcing F_{sgs_λ} can be quantified from the tendencies directly generated by the turbulent mixing scheme (or PBL scheme), which were added in the HWRF output in our experiments. Figure 10 compares the SGS tangential eddy forcing averaged over the RI period from 06 UTC 28 to 06 UTC 29 August, 2015 between the two HWRF simulations, where the upper and

5   bottom panels show the azimuthal-mean radial-height structure of SGS tangential eddy forcing and its horizontal plane view at 3 km altitude, respectively. There are a couple of interesting features shown in the figure. First, as expected, the in-cloud turbulent mixing parameterization allows HWRF to successfully generate the SGS tangential eddy forcing associated with the eyewall and rainband convection above the PBL (Figs. 10b and 10d), in contrast to virtually zero SGS eddy forcing above the PBL in DEF-HWRF (Figs. 10a and 10c). Second, in addition to the expected strong negative SGS tangential eddy

10   forcing within the PBL, the in-cloud turbulent mixing generates an interesting vertical structure of SGS tangential eddy forcing above the PBL in the eyewall. Although it is much weaker than that in the PBL, the SGS tangential eddy forcing in the eyewall does show positive values at the heights just above the inflow layer as well as above the mid troposphere, suggesting that the eyewall SGS tangential eddy forcing above the PBL is directly involved in the vortex spin-up processes during the RI. What remains unclear is the fidelity of the parameterized SGS eddy forcing above the PBL and its sensitivity

15   to specific turbulent mixing parameterization. This constitutes one of the uncertainties in storm intensity simulation.

The model-resolved tangential eddy forcing averaged over the RI period from 06 UTC 28 to 06 UTC 29 August, 2015 is shown in Fig. 11. The basic vertical and horizontal structures of the resolved eddy forcing generated by the two simulations are similar to a certain extent, but the eddy forcing is much stronger in TL-HWRF. A robust feature shown in both simulations is the positive eddy forcing right above the inflow layer in the vicinity of the eyewall. From the perspective of

20   absolute angular momentum conservation, this positive tangential eddy forcing is directly linked to the vortex spin-up. But currently we have little knowledge on what determines the sign, magnitude, and vertical structure of eddy forcing. Future research should focus on elucidating these issues regarding how eyewall and rainband eddy processes govern the TC intensification.

Comparing Fig. 11b with Fig. 10b, it is easy to see that the model-resolved eyewall eddy forcing above the PBL in the "TL-

25   HWRF" experiment has a magnitude about 5 times larger than the corresponding SGS eddy forcing, suggesting that the resolved eddy processes provide a major forcing that drives the primary circulation of the TC vortex in this case. As model resolution keeps increasing, we expect that the resolved eddy forcing will become more dominant. This is certainly a promising result, implying that numerical forecast of TC intensification may be ultimately a resolution problem. The difficulty, however, stems from the strong dependence of model-resolved eddy forcing on the parameterized SGS eddy

30   processes at the current resolution. As we showed in Figs. 8, 9, and 11, the only modification in SGS turbulent mixing parameterization in the eyewall and rainbands result in substantial differences in the vortex inner-core structure and the associated model-resolved eyewall/rainband eddy forcing. Such a dependence of the TC inner-core structure and model-

resolved eddy forcing on the parameterization of SGS in-cloud turbulence is not a surprise, since the large energy-containing turbulent eddies are not resolved at the current model resolution of 2 km. The strong dependence of the resolved TC vortex on SGS parameterization poses a great challenge for accurate prediction of TC intensity change.

The results presented previously show that eyewall/rainband eddy forcing plays a key role in Jimena's RI and the inclusion
5   of parameterization of eyewall/rainband in-cloud turbulent mixing above the PBL substantially improves HWRF's skills on generating robust eddy forcing for accurate intensity prediction. Such an improvement is not a special case, but is shown in HWRF simulations of other major TCs as well. Figure 12 shows the HWRF simulated maximum wind speed and storm central pressure of other 4 major hurricanes compared with the best track data. In all cases, the intensity simulations were improved due to the inclusion of in-cloud turbulent mixing parameterization, in particular, TL-HWRF was able to partially
10 capture the observed RI of Harvey (2017) and Marie (2014), which was largely missed by DEF-HWRF. Similar to the HWRF simulations of Jimena (2015), our analyses show that the better intensity forecasts of these storms by TL-HWRF can be largely attributed to the improved simulation of storm inner-core structure and eyewall/rainband eddy forcing needed for TC vortex spin-up. As another example, Figure 13 compares the satellite observed vortex inner-core structure of Harvey (2017) with the simulated ones by the two HWRFs during the early and middle stages of Harvey's RI. The asymmetric
15 rainband structure, the closed ring feature around the storm center, and the size of the convective ring shown in satellite observations are reasonably reproduced by TL-HWRF. But DEF-HWRF was not able to simulate the observed inner-core structure; in particular, it fails to generate the closed ring feature around the storm center. This result once again indicates that at the current model resolution, the storm structure and model-resolved eyewall/rainband eddy forcing that directly drives the primary and secondary circulation of a TC vortex are sensitive to the parameterized SGS eddy processes above the
20 PBL in the eyewall and rainbands.

Our testing simulations also show that the inclusion of in-cloud turbulent mixing parameterization in the eyewall and rainbands does not appear to degrade HWRF's performance on those cases that operational HWRF has decent forecasts on or generate false RI for those weak storms. As an example, Figure 14 shows the storm intensity of Hermine (2016) simulated by the two HWRFs compared with the best track data. Hermine (2016) is a weak storm with the peak intensity just reaching
25 Category-1 hurricane strength. The simulation results show that the integrated turbulent mixing parameterization in the eyewall and rainbands only has a marginal impact on the HWRF predicted storm intensity. It did not over-predict storm intensity or generate false RI that one may concern about.

4. Summary

From the perspective of absolute angular momentum conservation, this study argues that the success of numerical prediction
30 of TC intensity change largely depends on the skills of a model to generate appropriate eddy forcing that drives the primary and secondary circulations of a TC, provided that the model simulates the right SST and large-scale flow in which the TC

vortex is embedded. Because of the finite grid spacing of a model, the eddy forcing is split into two parts resulting from the model-resolved and parameterized SGS eddy processes. While higher model resolution allows the model-resolved eddy forcing to be better resolved, the parametric determination of SGS eddy forcing is source of uncertainty in storm intensity prediction.

5   In numerical simulations, the SGS eddy forcing is determined by the turbulent mixing scheme. Turbulence is commonly regarded as a flow feature of the PBL, and thus, a turbulent mixing scheme is also known as a PBL scheme in literature. In fair-weather conditions, indeed, the turbulent PBL is often cleanly separated from the free atmosphere above by a capping inversion. Except for occasional clear-sky turbulence, turbulent mixing is negligible above the PBL. The various PBL schemes used today in the state-of-the-art numerical models were designed to best represent the turbulent transport within

10 the PBL. In a TC environment, however, turbulence is no longer solely generated by the shear production and buoyancy production associated with the PBL processes. Intense turbulent mixing can also be generated by cloud processes above the PBL in the eyewall and rainbands due to radiative cooling, evaporative cooling, and inhomogeneous diabatic heating and cooling. While the concept of PBL is still applicable in the eyewall and rainbands as to the layer that is directly affected by the surface turbulent processes, the treatment of turbulent mixing must go beyond the conventional scope of the PBL. This is

15 particularly true in the TC inner-core region as air parcels ascend swiftly within the eyewall and rainbands where there is no physical interface that separates the turbulence generated by the PBL processes and cloud processes aloft. The conventional vortex PBL theory is, thus, insufficient to explain TC intensification, in particular rapid intensification, governed by TC internal eddy processes. Such a deficiency of classic PBL theory is reflected in the PBL scheme used in HWRF. The HWRF PBL scheme is a typical first-order K-closure scheme that parameterizes turbulent mixing based on the diagnosed PBL

20 height. Our analyses show that an artificial separation of the PBL from the free atmosphere above cannot appropriately represent the vertical turbulent structure in the eyewall and rainbands, in particular, the simple method of parameterizing turbulent mixing above the PBL based on the bulk Richardson number is unable to account for the intense turbulent mixing aloft generated by eyewall/rainband cloud processes. As a result, the HWRF PBL scheme fails to generate the eyewall/rainband SGS eddy forcing needed for driving the primary and secondary circulation of a TC vortex.

25 In this study, we developed a method to allow for an integrated turbulent mixing parameterization in the eyewall and rainbands based on the "TL" determined by the simulated radar reflectivity. Such a change from "PBL" to "TL" will not affect the turbulent mixing parameterization outside the eyewall and rainbands since the "TL" is virtually the same as "PBL" in non-convective regions. This simple adjustment allows HWRF to successfully generate eyewall/rainband SGS eddy forcing above the PBL. Numerical tests on multiple major hurricanes show that the inclusion of in-cloud turbulent mixing

30 parameterization notably improves HWRF's skills on predicting TC intensity change, in particular, RI. While the performance of the modified turbulent mixing scheme is promising, our treatment of in-cloud turbulent mixing itself is very crude, and thus, the scheme may not be ready for use in operational TC forecasts in its current form. Nonetheless, our results show that numerical simulations of TC intensification are sensitive to the SGS eddy forcing of eyewall and rainbands. Future

research should focus on developing physically robust scheme to better represent in-cloud turbulent processes and advance our theoretical understanding of how eyewall/rainband eddy forcing above the PBL modulates TC intensification including RI. There are scientific questions that need to be further addressed and clarified, such as, what determines the sign, magnitude, and vertical distribution of eyewall/rainband forcing? And is eddy forcing that leads to TC intensification a

5   stochastic process or deterministic process?

While the improvement of TC intensity forecast due to the inclusion of in-cloud turbulent mixing parameterization is clearly demonstrated, the underlying reason for such an improvement appears to be complicated. At first glance, the calculated SGS eddy forcing above the PBL is about five times smaller than the model-resolved eddy forcing (Figs. 10b and 11b). This would suggest that the model-resolved eddy forcing is the dominant forcing for the spin-up of the TC vortex at the current

10   model resolution. However, the simulated TC inner-core structure and the associated model-resolved eddy forcing show a strong dependence on the parameterized SGS eddy processes. This result suggests that the model-resolved and SGS eddy forcings are not independent, although they appear as two separate terms in the governing equations and are determined separately in numerical simulations. Such a dependence is understandable since large energy-containing turbulent eddies are not resolved but parameterized at a grid spacing of 2 km. Will further increasing of model resolution reduce the dependence

15   of model-resolved eddy forcing on SGS processes? Likely not, unless energy-containing eddies can be resolved and the model-resolved eddy forcing is approved to be insensitive to turbulence with scales smaller than the inertial subrange. To do so, large-eddy resolution both horizontally and vertically is needed not only in the PBL (like classic LES) but also aloft in the eyewall and rainbands to resolve in-cloud turbulence generated by cloud processes. This is not likely to happen in the near future for operational forecasts even with ever-increasing computational capability. Therefore, as model resolution

20   keeps increasing, research effort should be continuously devoted to improving parametric representation of model physics not only in the PBL but also above the PBL to appropriately account for microphysical processes, in-cloud turbulent processes, and the interaction among microphysics, dynamics, and turbulence.

Acknowledgement

This work is supported by NOAA/HFIP under Grants NA14NWS4680030 and NA16NWS4680029, National Science

25   Foundation under Grant AGS-1822238 and AGS-1822128, and BP/The Gulf of Mexico Research Initiative. All data used in this study can be accessed at http://vortex.ihrc.fiu.edu/download/HWRF-TUR/.

References

Aligo, E. A., Ferrier, B., and Carley, J. R.: Modified NAM Microphysics for Forecasts of Deep Convective Storms. Mon. Wea. Rev., doi:10.1175/MWR-D-17- 0277.1, in press.

Arakawa, A., and Schubert, W. H.: Interaction of a cumulus cloud ensemble with the large-scale environment: Part I. J. Atmos. Sci., 31, 674–701, 1974.

Bui, H. H., Smith, R. K., Montgomery, M. T., and Peng, J.: Balanced and unbalanced aspects of tropical cyclone intensification. Quart. J. Roy. Meteor. Soc., 135, 1715–1731, DOI: 10.1002/qj.502, 2009.

5   Businger J. A., Wyngaard, J. C., Izumi, I., Bradley, E. F.: Flux-profile relationships in the atmospheric surface layer. J. Atmospheric Sci. 28, 181-189, 1971.

Charney, J. G. and Eliassen, A.: On the growth of the hurricane depression. J. Atmos. Sci., 21, 68-75, 1964.

Deardorff, J. W.: Parameterization of the planetary boundary layer for use in general circulation models. Mon. Wea. Rev. 100, 93-106, 1972.

10   Emanuel, K. A.: An air-sea interaction theory for tropical cyclones. Part I: Steady state maintenance. J. Atmos. Sci., 43, 585-604, 1986.

Giangrande, S. E., Collis, S., Straka, J., Protat, A., Williams, C., and Krueger, S.: A summary of convective-core vertical velocity properties using ARM UHF wind profilers in Oklahoma. J. of Appl. Meteor. Climat., 52, 2278–2295, 2013.

Gopalakrishnan, S., Marks, F. D., Zhang, J. A., Zhang, X., Bao, J.-W., and Tallapragada, V.: A study of the impact of
15   vertical diffusion on the structure and intensity of tropical cyclones using the high-resolution HWRF system. J. Atmos. Sci. 70, 524-541, 2013.

Hogan, R. J., Grant, A. L. M., Illingworth, A. J., Pearson, G. N., and O'Connor, E. J.: Vertical velocity variance and skewness in clear and cloud-topped boundary layers as revealed by Doppler lidar. Quart. J. Roy. Meteor. Soc., 135, 635–643, 2009.

20   Holtslag, A. A. M, de Bruijn, E. I. F., and Pan, H.-L.: A high-resolution air mass transformation model for short-range weather forecasting. Mon. Wea. Rev., 118, 1561–1575, 1990.

Holtslag, A. A. M, and Boville, B. A.: Local versus nonlocal boundarylayer diffusion in a global model. J. Climate, 6, 1825–1842, 1993.

Hong, S.-Y., and Pan, H.-L: Nonlocal boundary layer vertical diffusion in a Medium-Range Forecast model. Mon. Wea.
25   Rev., 124, 2322–2339, 1996.

Jiang, H., and Ramirez, E. M.: Necessary conditions for tropical cyclone rapid intensification as derived from 11 years of TRMM data. J. Climate., 26, 6459-6470, 2013.

Kieper, M. E., and Jiang, H.: Predicting tropical cyclone rapid intensification using the 37GHz ring pattern identified from passive microwave measurements. Geophys. Res. Lett., 39, L13804, dio: 10.1029/2012GL052115, 2012.

30   Kleinschmidt, K.: Grundlagen einer Theorie der tropischen Zyklonen. Arch. Meteor. Geophys. Bioklim., A4, 53–72, 1951.

LeMone, M. A. and Zipser, E. J.: Cumulonimbus vertical velocity events in GATE. Part I: Diameter, intensity and mass flux, J. Atmos. Sci., 37, 2444–2457, 1980.

Lorsolo, S, Zhang, J. A., Marks, F. D., and Gamache, J.: Estimation and mapping of hurricane turbulent energy using airborne Doppler measurements. Mon. Wea. Rev., 138, 3656-3670, 2010.

Marks, F. D., Black, P. G., Montgomery, M. T., and Burpee, R. W.: Structure of the eye and eyewall of Hurricane Hugo (1989), Mon. Wea. Rev., 136, 1237–1259, 2008.

Marks, F. D. and Shay, L. K.: Landfalling tropical cyclones: Forecast problems and associated research opportunities. Bull. Amer. Meteor. Soc., 79, 305-323, 1998.

Montgomery, M. T. and Smith, R. K.: Paradigms for tropical cyclone intensification. Australian Meteorological and Oceanographic Journal, 64, 37–66, 2014.

Moss, M. S, and Rosenthal, S. L.: On the estimation of planetary boundary layer variables in mature hurricanes. Mon. Wea. Rev. 103, 980–988, 1975.

Nolan, D. S., Moon, Y., and Stern, D. P.: Tropical cyclone intensification from asymmetric convection: Energetics and efficiency. J. Atmos. Sci., 64, 3377-3405, 2007.

Ooyama K. V.: Conceptual evolution of the theory and modeling of the tropical cyclone. J. Meteor. Soc. Japan, 60, 369–80, 1982.

Riehl, H.: Tropical meteorology. McGraw-Hill, 392pp, 1954.

Shapiro, L.: The asymmetric boundary-layer flowunder a translating hurricane. J. Atmos. Sci,. 40, 1984–1998, 1983.

Shapiro, L. J., and Willoughby, H. E.: The response of balanced hurricanes to local sources of heat and momentum. J. Atmos. Sci., 39, 378–394,

doi: 10.1175/1520-0469(1982)039<0378:TROBHT>2.0.CO;2, 1982.

Smith, R. K, Montgomery, M. T., and Vogl, S.: A critique of Emanuel's hurricane model and potential intensity theory. Q. J. R. Meteorol. Soc., 134: 551–561, 2008.

Smith, R. K, Montgomery, M. T., and Zhu, H.: Buoyancy in tropical cyclones and other rapidly rotating atmospheric vortices. Dynamics of Atmospheres and Oceans, 40, 189-208, 2005.

Smith, R. K, and Montgomery, M. T.: Hurricane boundary layer theory. Q. J. R. Meteorol. Soc. 136, 1665–1670, 2010.

Stull, R. B.: An introduction to boundary-layer meteorology. Kluwer: Dordrecht, The Netherlands, 670pp, 1988.

Tao, C., and Jiang, H.: Distributions of shallow to very deep precipitation–convection in rapidly intensifying tropical cyclones. J. Climate, 28, 8791–8824. doi:http://dx.doi.org/10.1175/JCLI-D-14-00448.1, 2015.

Troen, I., and Mahrt, L.: A simple model of the atmospheric boundary layer: Sensitivity to surface evaporation. Bound.-Layer Meteor., 37, 129–148, 1986.

Wu, C.-M., and Arakawa, A.: A Unified Representation of Deep Moist Convection in Numerical Modeling of the Atmosphere. Part II. J. Atmos. Sci., 71, 2089-2103, 2014.

Zhang J. A., Marks , F. D., Montgomery, M. T., and Lorsolo, S.: An estimation of turbulent characteristics in the low-level region of intense Hurricanes Allen (1980) and Hugo (1989). Mon. Wea. Rev., 139, 1447–1462, 2011.

Zhu, P., Wang, Y., Chen, S. S., Curcic, M., Gao, C.: Impact of storm-induced cooling of sea surface temperature on large turbulent eddies and vertical turbulent transport in the atmospheric boundary layer of Hurricane Isaac, J. Geophys. Res. - Oceans, 121, 861-876, doi:10.1002/2015JC011320, 2015.

Zhu, P.: Simulation and parameterization of the turbulent transport in the hurricane boundary layer by large eddies. J. Geophys. Res., 113, D17104, doi:10.1029/2007JD009643, 2008.
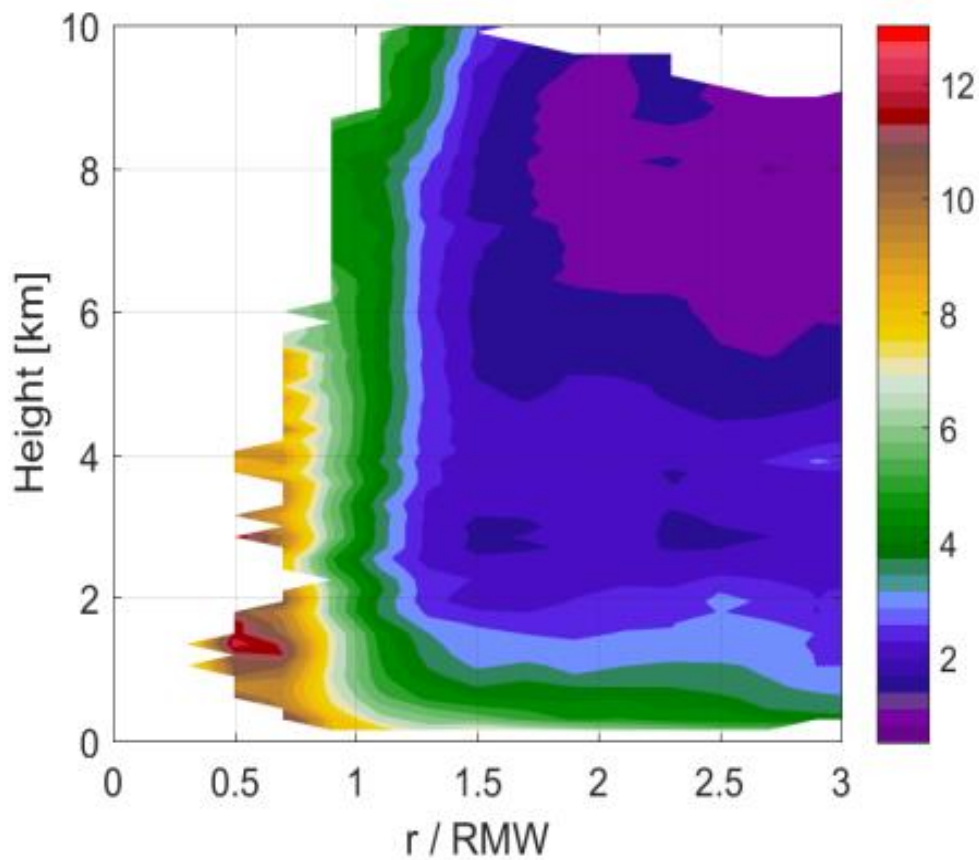
Figure 1: Composite TKE derived from airborne radar data from 116 radial legs of P3 flights in the 2003-2010 hurricane seasons as a function of height and the radius normalized by the radius of maximum wind (RMW).
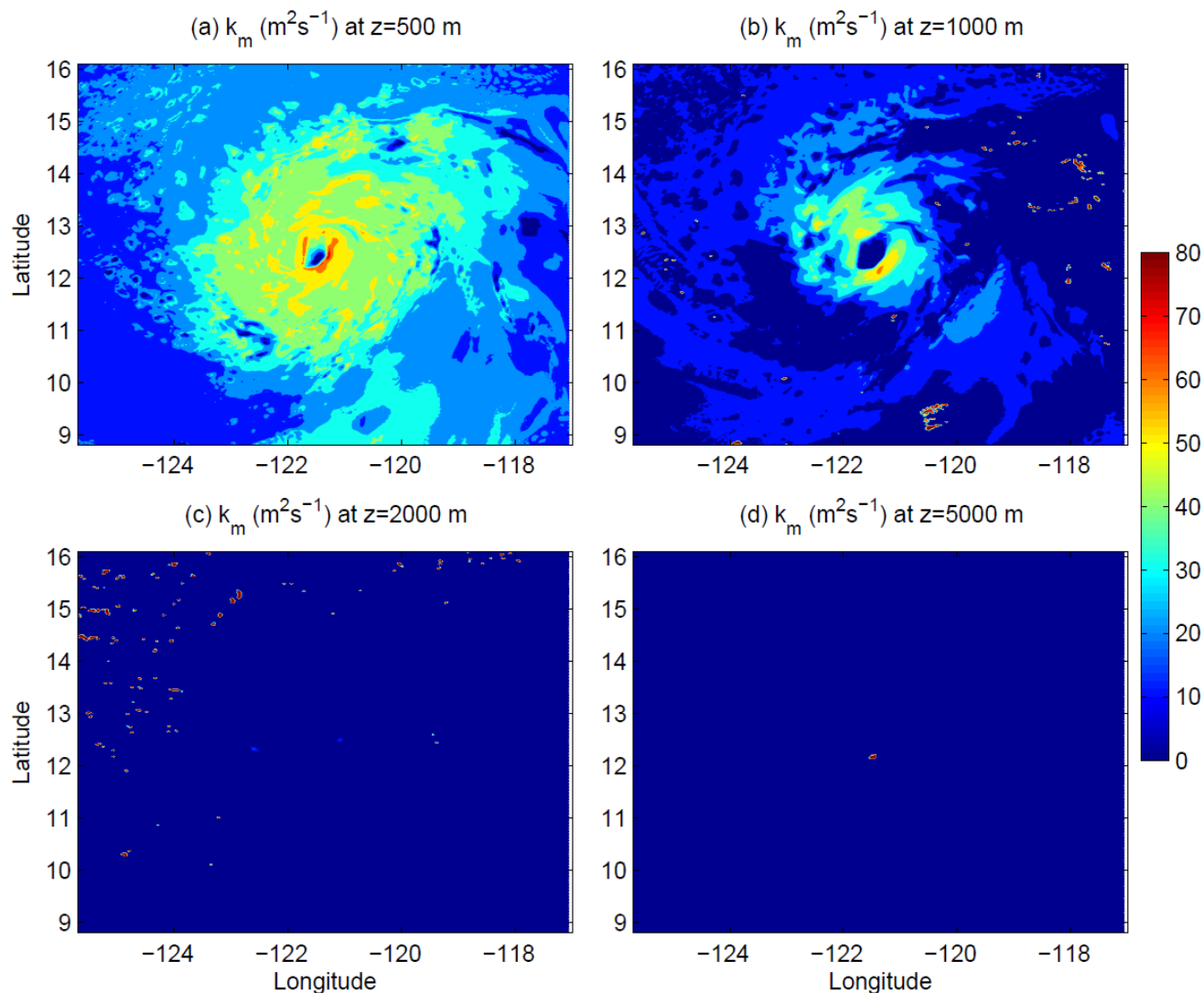
Figure 2: Eddy exchange coefficients of momentum at different altitudes (z = 0.5, 1.0, 2.0, and 5.0 km) from a HWRF simulation of Hurricane Jimena (2015) at 12:00 UTC 28 August, 2015.
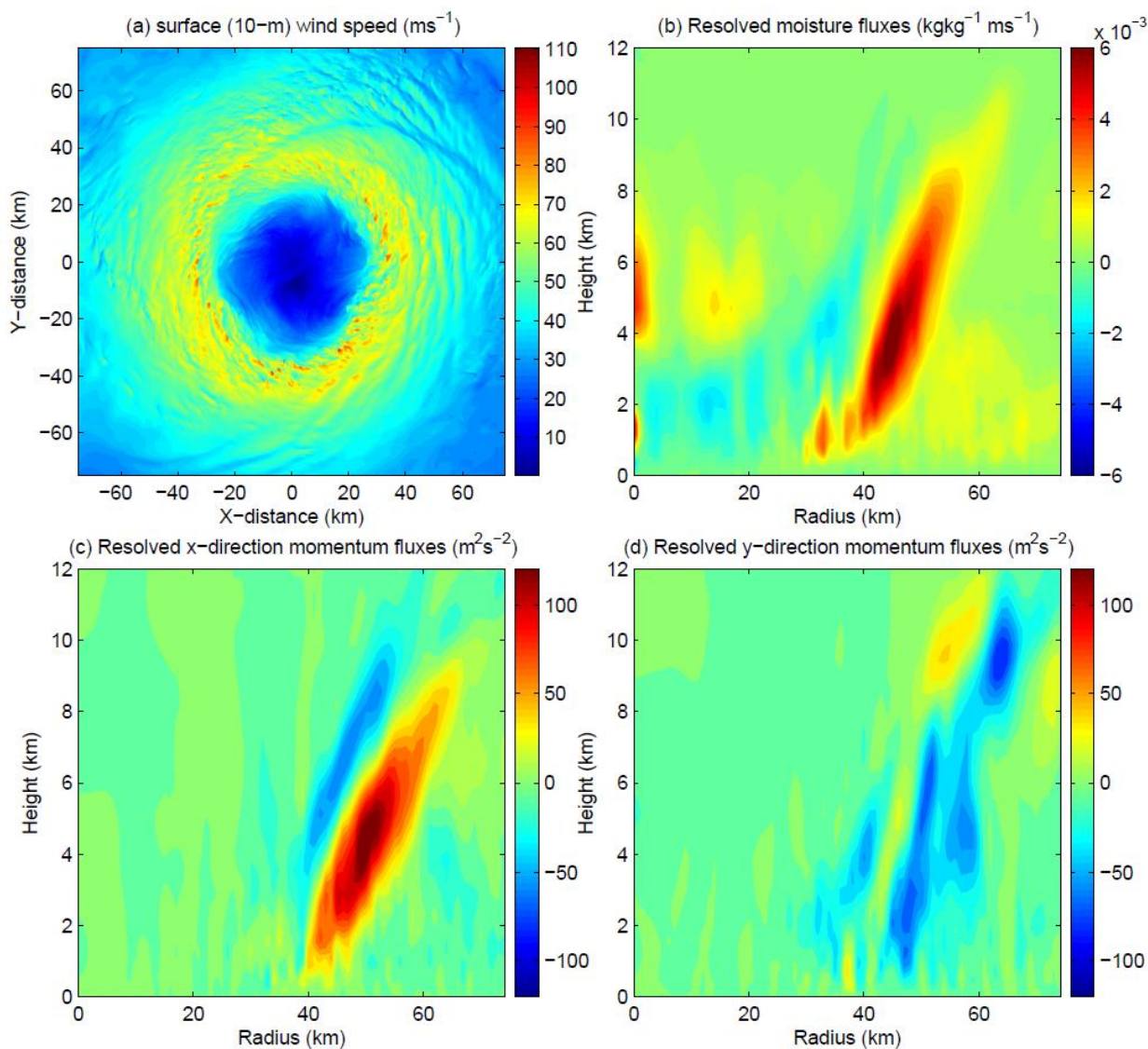
Figure 3: (a): 10-m surface wind speeds of Hurricane Isabel (2003) simulated by a LES with horizontal grid spacing of 100 m after 8 simulation hours. (b): Azimuthal-mean radius-height structure of LES-resolved kinematic moisture fluxes $(\overline{w'q'})$ determined by the eddy correlation method after 8 simulation hours. (c): The same as (b) but for x-direction kinematic momentum fluxes $(\overline{w'u'})$. (d): The same as (b) but for y-direction momentum fluxes $(\overline{w'v'})$.
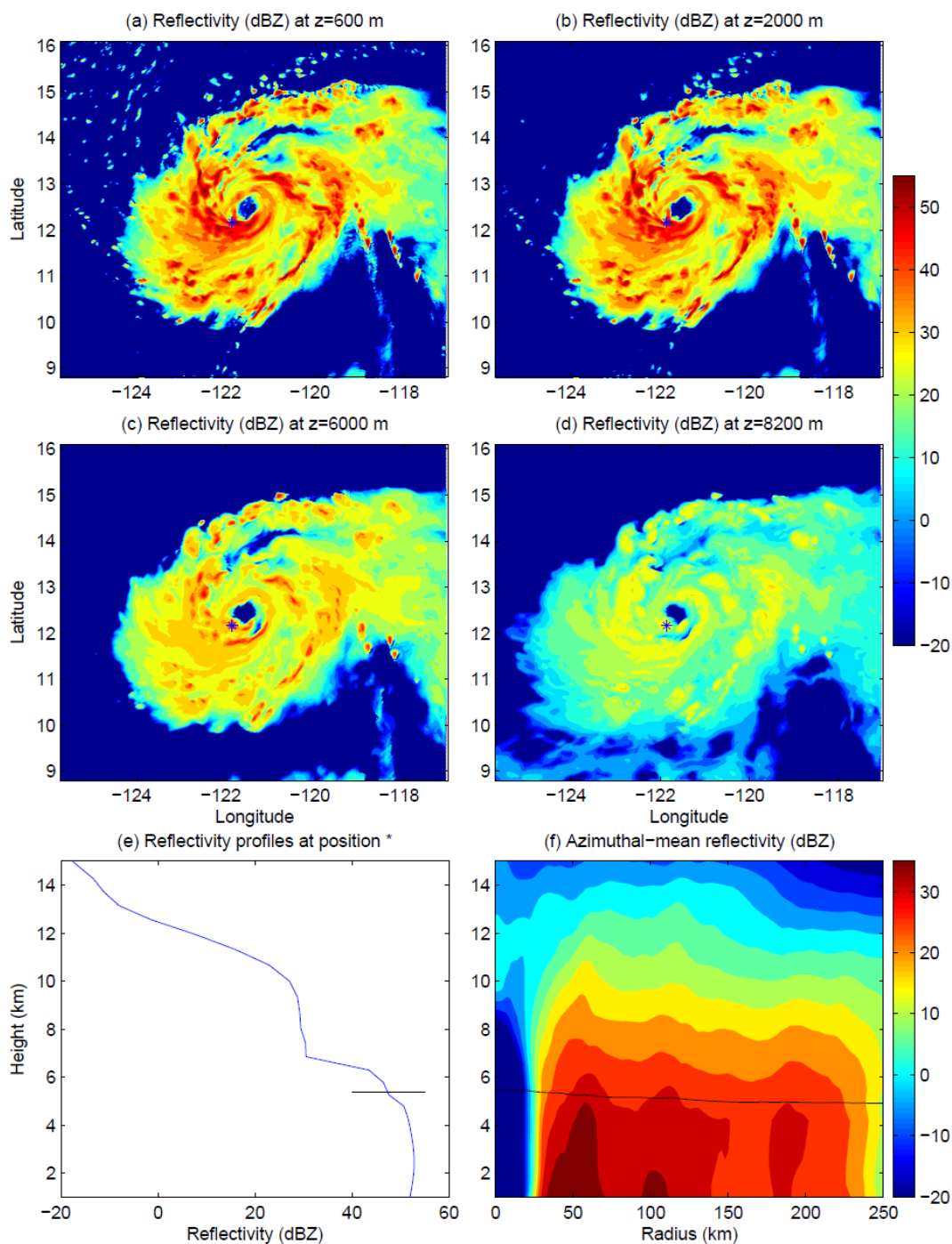
Figure 4: (a)-(d): HWRF simulated radar reflectivity of Hurricane Jimena (2015) at different altitudes (z = 0.6, 2.0, 6.0, and 8.2 km) at 12:00 UTC 28 August, 2015. (e): Vertical profile of radar reflectivity at a location in the eyewall marked by "*" in (a)-(d). (f): Azimuthal-mean radius-height structure of radar reflectivity. Black line in (e) and (f) indicates the freezing line.
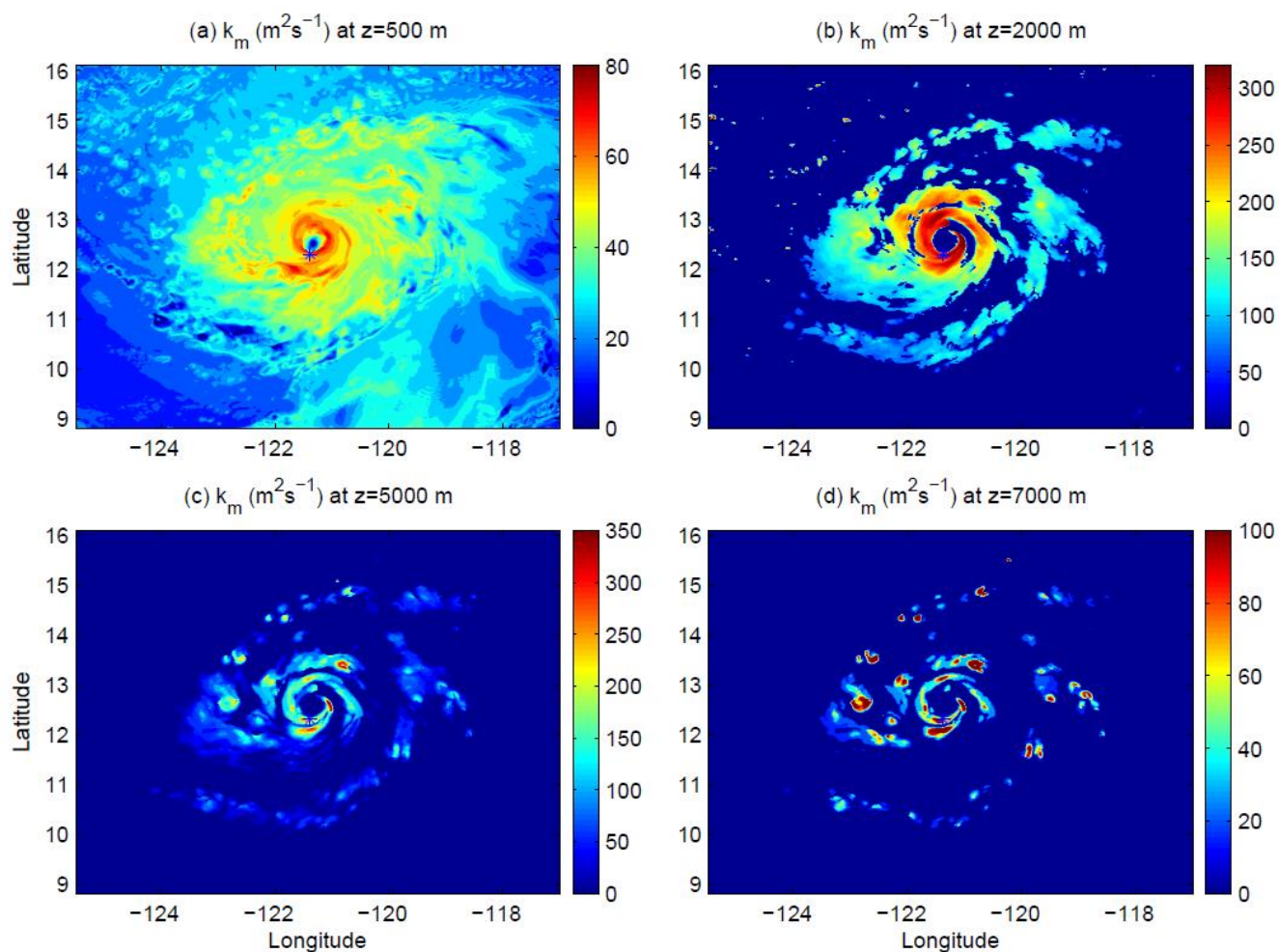
Figure 5: Simulated eddy exchange coefficient of momentum (k_m) at different altitudes (z = 0.5, 2.0, 5.0, and 7.0 km) at 12:00 UTC 28 August, 2015 from the HWRF with the inclusion of in-cloud turbulent mixing parameterization (TL-HWRF).
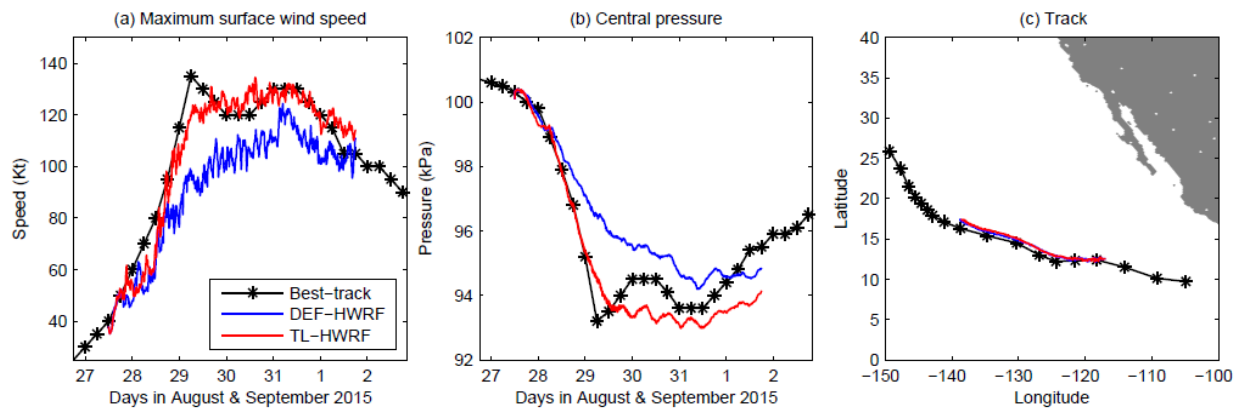
Figure 6: Comparison of HWRF simulated maximum surface wind speed, storm central pressure, and track of Jimena (2015) with the best track data (Black). Blue curve indicates the simulation by the default HWRF (DEF-HWRF). Red curve indicates the simulation by the HWRF with inclusion of in-cloud turbulent mixing parameterization (TL-HWRF).
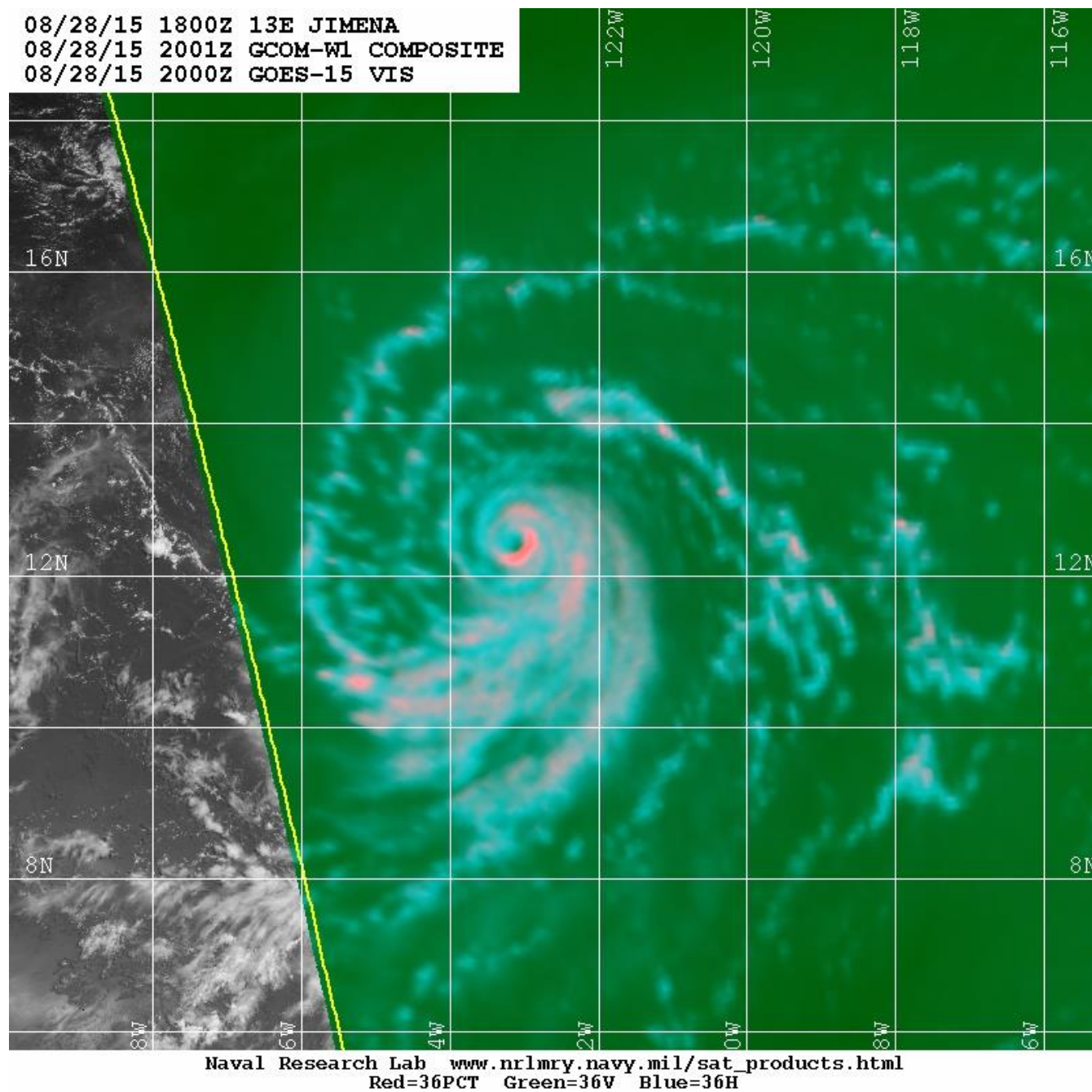
Figure 7: Naval Research Laboratory 37 GHz color image from the Advanced Microwave Scanning Radiometer 2 (AMSR2) at 20:00 UTC 28 August, 2015.
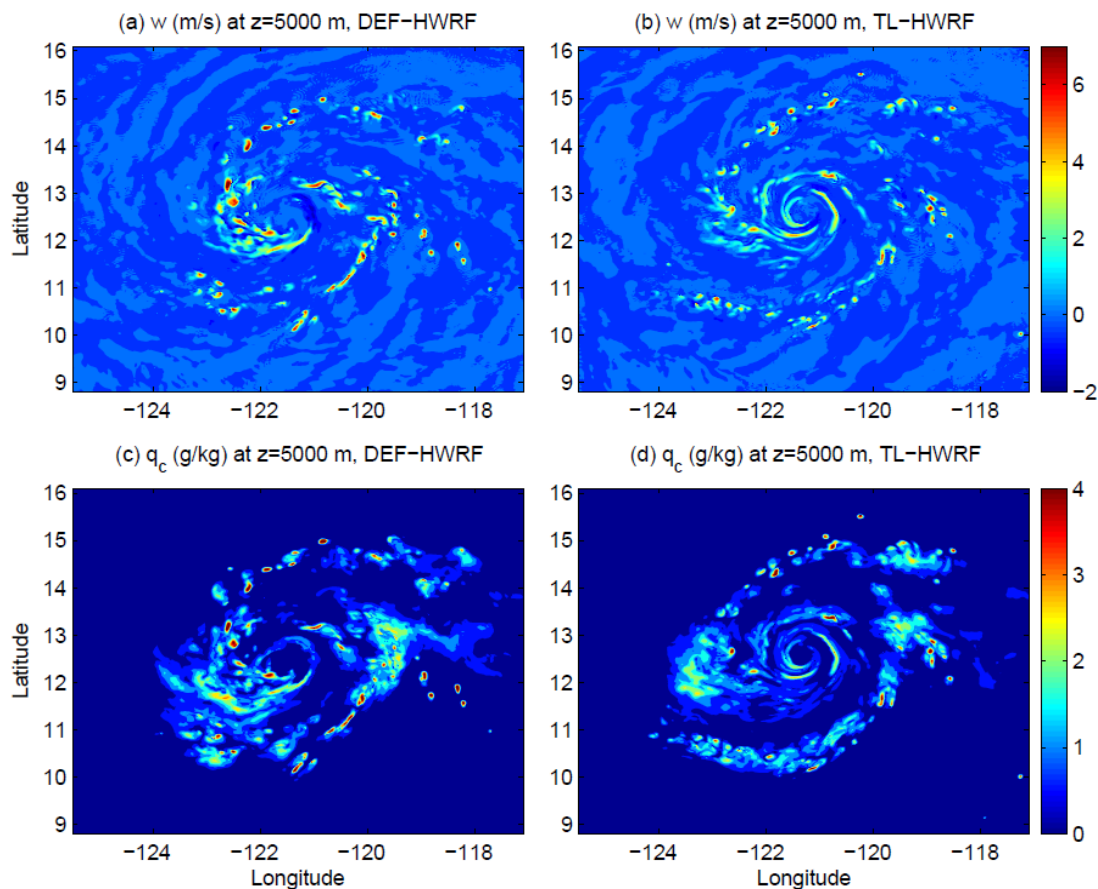
Figure 8: Simulated vertical velocity (ms^{-1}) and hydrometeor mixing ratio (gkg^{-1}) at 5.0 km altitude at 12:00 UTC 28 August, 2015 by the default HWRF (DEF-HWRF) and the HWRF with the inclusion of in-cloud turbulent mixing parameterization (TL-HWRF).
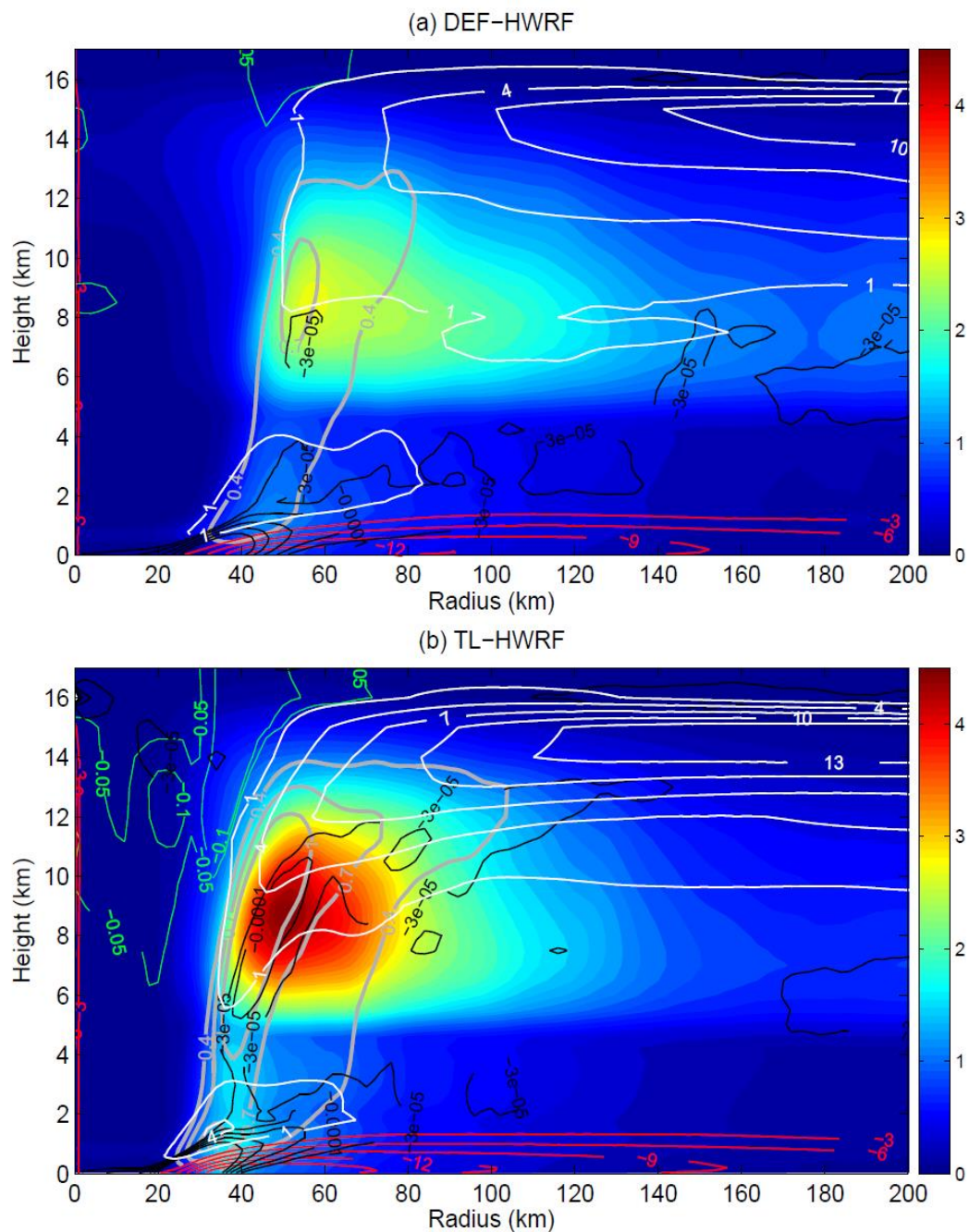
Figure 9: Simulated azimuthal-mean radius-height structure of updrafts (grey contours, ms^{-1}), downdrafts (green contours, ms^{-1}), hydrometeor mixing ratio (color shading, gkg^{-1}), radial inflow (red contours, ms^{-1}), outflow (white contours, ms^{-1}), and radial flow convergence (black contours, s^{-1}) averaged over Jimena's RI period from 06:00 UTC 28 to 06:00 UTC 29 August, 2015.
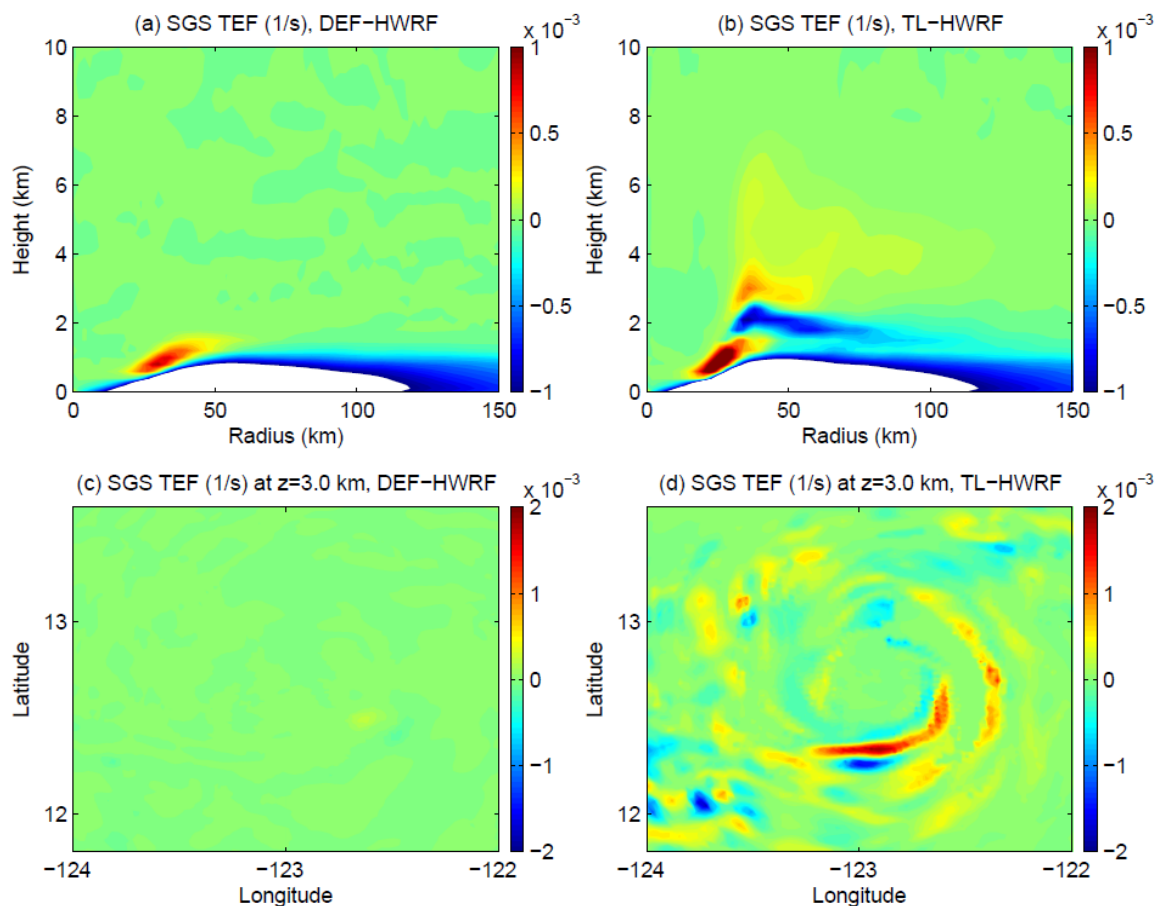
Figure 10: SGS tangential eddy forcing (TEF) averaged over Jimena's RI period from 06:00 UTC 28 to 06: UTC 29 August, 2015 from the two HWRF simulations (DEF-HWRF and TL-HWRF). Top panels: azimuthal-mean radius-height structure of SGS TEF. Note that the SGS TEF smaller than -1.0e-3 (s^{-1}) is shaded with white color for a clear illustration of SGS TEF above the PBL. Bottom panels: horizontal structure of SGS TEF at 3 km altitude.
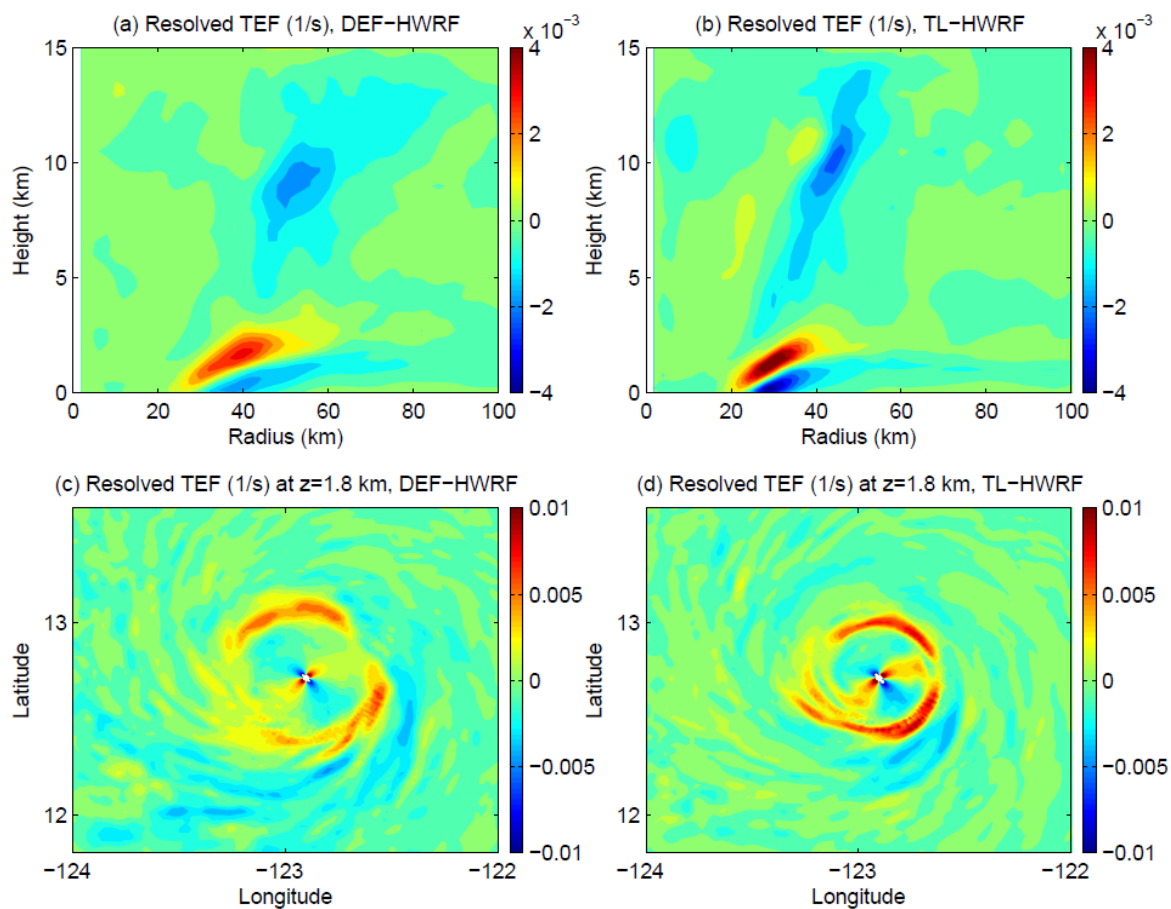
Figure 11: Model-resolved tangential eddy forcing (TEF) averaged over Jimena's RI period from 06:00 UTC 28 to 06:00 UTC 29 August, 2015 from the two HWRF simulations (DEF-HWRF and TL-HWRF). Top panels: azimuthal-mean radius-height structure of resolved TEF. Bottom panels: horizontal structure of resolved TEF at 1.8 km altitude.
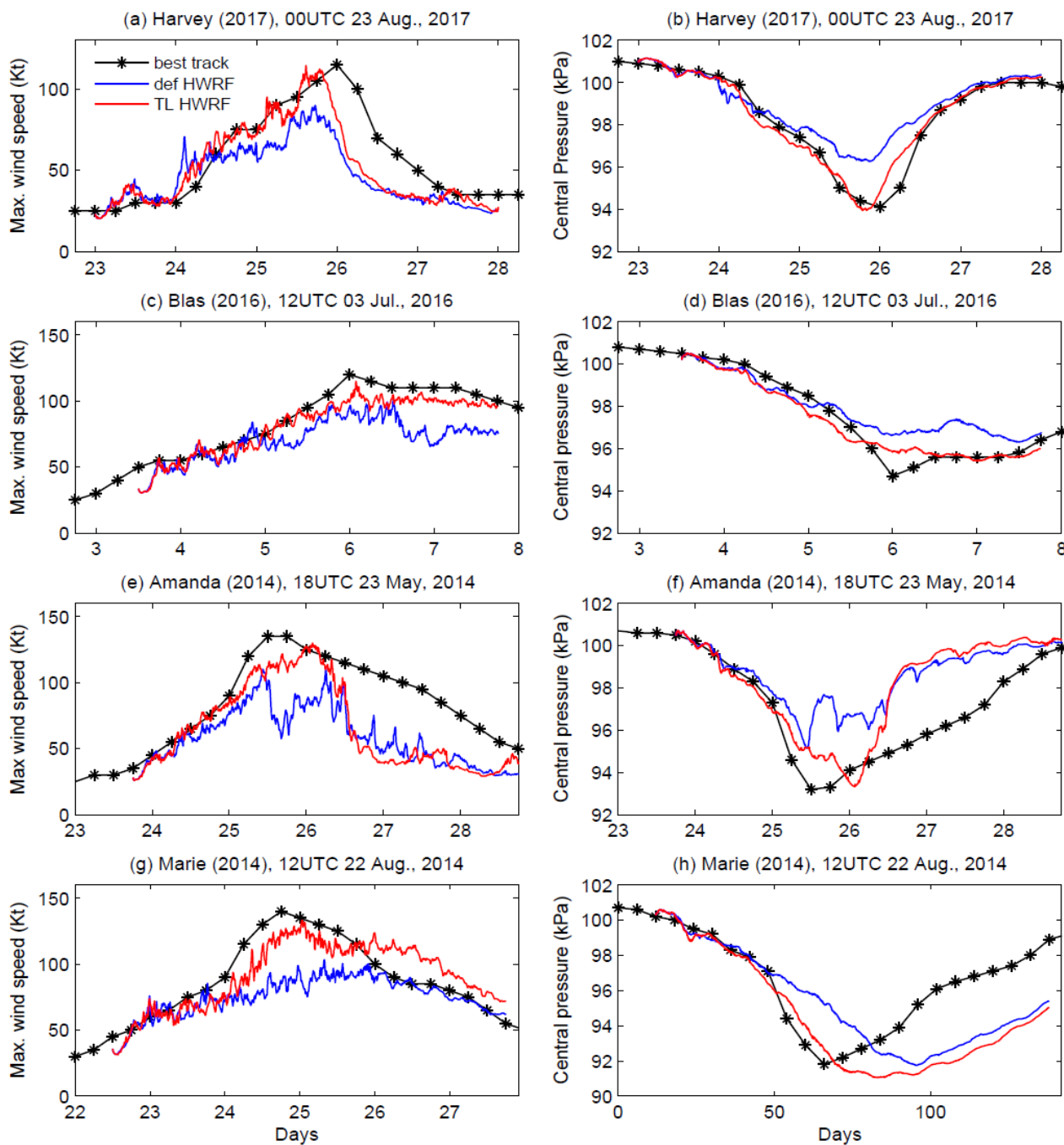
Figure 12: HWRF simulated maximum wind speed and storm central pressure of other 4 major hurricanes, Harvey (2017), Blas (2016), Amanda (2014), and Marie (2014), compared with the best track data (black curves). Blue curves: DEF-HWRF; Red curves: TL-HWRF.
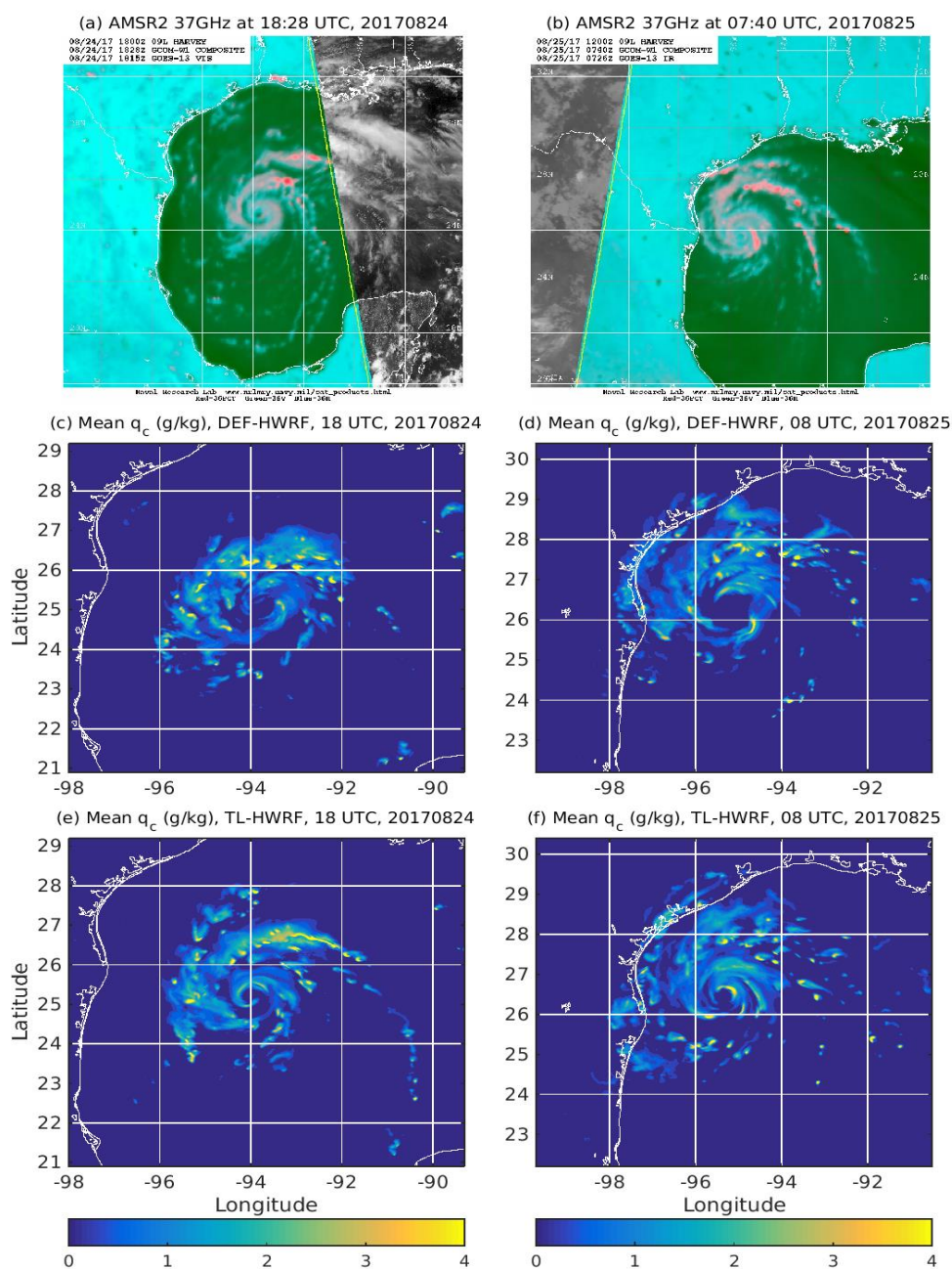
Figure 13: Comparison of vortex inner-core structure during the early stage (left column) and mid stage (right column) of Harvey (2017)'s RI between satellite (AMSR2) observations (top panels) at 18:28 UTC 24 and 07:40 UTC 25 August 2017 and HWRF simulations by DEF-HWRF (middle panels) and TL-HWRF (bottom panels) at 18:00 UTC 24 and 08:00 UTC

5   25 August 2017. The shown simulated fields are the hydrometeor mixing ratio (gkg^{-1}) at 5.0 km altitude.
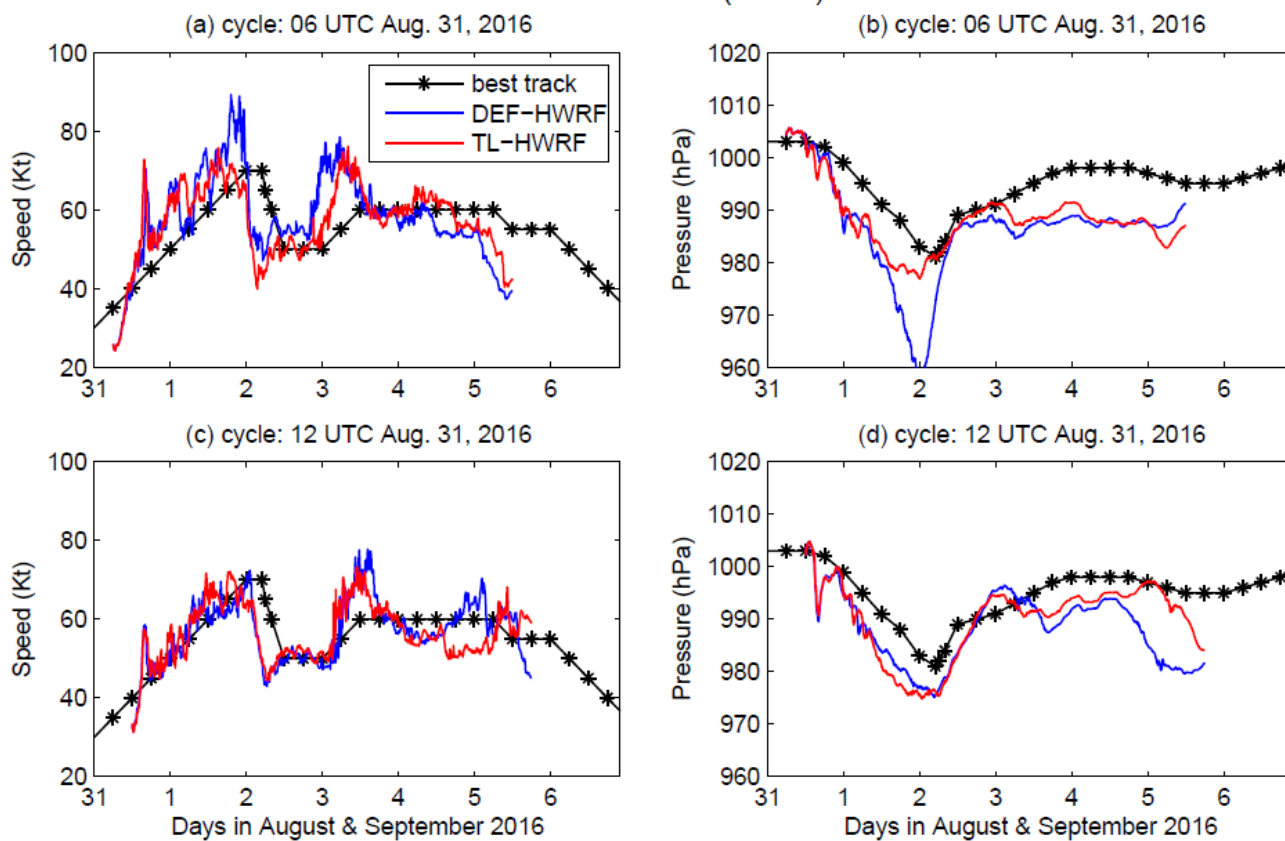
Figure 14: Comparison of HWRF simulated maximum surface wind speed, storm central pressure, and track of Hermine (2016) with the best track data (Black). Blue curves: DEF-HWRF. Red curves: TL-HWRF.